No. 5

Bin Cheng

On the modelling of sea ice thermodynamics and air-ice coupling in the Bohai Sea and the Baltic Sea

Cover: Theoretical vertical temperature profiles (blue lines) in the sea ice. The black broken lines denote the hypothetical temperature profiles if the melting condition is switched off. In the model such conditions indicate the surface and sub-surface melting with temperature limit as 0 °C. The arrows on the top indicate turbulent and radiative heat exchange at the surface. The horizontal lines show the model gird levels.

On the modelling of sea ice thermodynamics and air-ice coupling in the Bohai Sea and the Baltic Sea

Bin Cheng

CONTENTS

NOTATION

T	temperature
V	wind speed
Rh	relative humidity
C	cloudiness factor
h	thickness of ice or snow
ρ	density
c	specific heat
k	heat conductivity
s	salinity
(L_f)	latent heat of fusion
L_v	enthalpy of vaporization
κ	extinction coefficient
α	surface albedo
Q_s	incoming solar radiation
Q_0	downward solar radiation under clear sky conditions
q	penetrating solar radiation below surface
I_0	penetrating solar radiation below the surface layer
Q_d	downwelling long-wave radiation
Q_b	upwelling long-wave radiation
Q_h	sensible heat flux
Q_{le}	latent heat flux
F_c	surface conductive heat flux
F_m	heat flux due to surface melting
F_w	oceanic heat flux
z	vertical coordinate in ice model positive downwards
z_a	vertical coordinate in the ABL model positive upward
za	height of za in the air
t	time

S	solar constant
Z	zenith angle
ε	surface emissivity
σ_a	Stefan-Boltzmann constant
k_0	von Karman constant
g	acceleration due to gravity
R	gas constant,
f	Coriolis parameter
Ri	Richardson number
C_H	exchange coefficient for heat
C_E	exchange coefficient for moisture
$u*$	fraction velocity
τ	momentum flux
z_0	roughness lengths for wind
z_T	roughness lengths for temperature
z_q	roughness lengths for moisture
q	specific himudity
Θ	potential air temperature
E	turbulent flux of water vapour (evaporation)
H	turbulent flux of sensible heat
L	Obukhov-length
ϕ	geopotential
p_s	surface pressure
p_t	pressure at the model top (3 km).
l	mixing length
c_p	specific heat of air
e	vapour pressure

subscripts:

a	air
s	snow
i	sea ice
sfc	surface
bot	ice bottom
w	water

ABBREVIATIONS

ABL	atmospheric boundary layer
BALTEX	Baltic Sea Experiment
BASIS	Baltic Air-Sea-Ice Study
CN	Crank-Nicholson scheme
FIMR	Finnish Institute of Marine Research
GEWEX	Global Energy and Water Cycle Experiment
IDA	Ice Data bank for Baltic Sea climate studies
NRCMEF	National research Centre for Marine Environmental Forecasts
WCRP	World Climate Research Programme

LIST OF ORIGINAL ARTICLES

The thesis is based on the following original articles, referred to in the text by Roman numerals:

I   Cheng, B., 1996. The conservative difference scheme and numerical simulation of a one-dimensional thermodynamic sea ice model. *Marine Science Bulletin*, 15(4): 8-15. (English translation of the original Chinese article)

II   Launiainen, J. and Cheng, B., 1998. Modelling of ice thermodynamics in natural water bodies. *Cold Regions Science and Technology*, 27: 153-178.

III   Cheng, B., Launiainen, J., Vihma, T. and Uotila, J. 2001. Modelling sea ice thermodynamics in BALTEX-BASIS. *Annales of Glaciology*, 33: 243-247.

IV   Launiainen, J., Cheng, B., Uotila, J. and Vihma, T. 2001. Turbulent surface fluxes and air-ice coupling in the Baltic-Air-Ice Study (BASIS). *Annales of Glaciology*, 33: 237-242.

V   Cheng, B., 2002. On the numerical resolution in a thermodynamic sea ice model. – Accepted to *Journal of Glaciology.*

VI   Cheng, B. and Vihma, T., 2002. Modelling of sea ice thermodynamics and air-ice coupling during warm-air advection. – Conditionally accepted to *Journal of Glaciology*.

Papers are reprinted with the kind permission of the Elsevier Science (paper **II**), the International Glaciological Society (papers **III**, **IV**, **V** and **VI**).

On the modelling of sea ice thermodynamics and air-ice coupling in the Bohai Sea and the Baltic Sea

Bin Cheng

Finnish Institute of Marine Research, P.O. Box 33,
FIN-00931 Helsinki, Finland

ABSTRACT

A one-dimensional thermodynamic sea ice model was constructed, in which different parameterizations of the surface radiative fluxes were studied and compared. The effect of atmospheric stratification was taken into account in the calculation of the turbulent surface heat fluxes based on the Monin-Obukhov similarity theory. A two-layer parameterization of penetrating solar radiation attenuating through the sea ice was introduced. The ice model solves the full heat conduction equation associated with heat fluxes and ice/snow mass moving boundaries. A conservative finite-difference numerical scheme of the heat conduction equation was derived using an integral interpolation method. This scheme was validated by numerical tests. The impact of numerical resolution on model predictions was studied. The ice model was coupled with a two-dimensional hydrostatic mesoscale atmospheric boundary layer (ABL) model to study the effect of warm-air advection on ice thermodynamics and the air-ice coupling.

The model was applied to study the ice thermodynamic processes in the seasonal ice cover of the Bohai Sea and the Baltic Sea. The model results were compared with field measurements. The model simulated various surface fluxes well, in particular the turbulent fluxes. The model also well reproduces the diurnal variation of ice temperature and seasonal evolution of ice thickness.

Process study using the Baltic Air-Sea-Ice Study (BASIS) field data suggested that during an ice thermal equilibrium stage the modelled superimposed ice formation gives a good estimation of the snow-ice formation. The model initialization is important for a short-term simulation. A sub-surface melting in early spring due to solar radiation absorption was also simulated.

The heat transfer coefficient and temperature roughness length were studied based on the analysis of the turbulent surface fluxes measured during BASIS. There was good mutual agreement with the surface temperature and the turbulent fluxes estimated by the eddy-flux and the gradient methods and the ice model.

The numerical scheme of the ice model was verified against analytical solutions. During the freezing season, the effect of numerical resolution on model results is not significant. When the downward short-wave radiation become large, the absorption of this flux below the ice or snow surface changes the predictions of ice temperature and surface heat fluxes in a way depending on the model spatial resolution chosen. A two-layer scheme for handling penetrating solar radiation in ice is suitable for a fine-resolution model.

During advection of warm air over an initially cold snow/ice layer, the air-ice turbulent heat flux has a direction opposite to the prevailing upward heat flux from the ocean through the snow/ice.

This results in a time-fetch and a time-depth dependent behaviour of the directionally-varying conductive heat flux in the snow/ice layer. From the point of view of ABL modelling, the interactive coupling between the air and ice was most important when the wind was strong, while from the point of view of ice thermodynamic modelling the coupling was most important when the wind was light.

---

1. INTRODUCTION

1.1 Background

71 % of the Earth's surface is covered by ocean, of which area some 7 % on the average is covered by sea ice. Sea ice belongs to the cryosphere and plays an important role in the global climate system via linkages and feedbacks generated through various processes (Fig. 1). Sea ice is a product of the thermodynamic interaction between the cold atmosphere and the underlying ocean. The ocean-atmosphere heat exchange is very sensitive to the thin portion of the sea ice thickness distribution (Maykut 1978, 1982). Sea ice acts as a barrier to the transfer of moisture, heat, and momentum between the atmosphere and the ocean. It is an effective heat sink for the atmosphere and ocean both through its high surface albedo and its large latent heat of freezing (Ebert & Curry 1993). In polar regions, the high surface albedo of sea ice reflects a large portion of the incoming solar radiation and reinforces the cooling of the atmosphere, providing a positive feedback to support the maintenance of the ice cover. The cooling of the atmosphere leads to strong meridional temperature gradients, and to an increase in the intensity of the zonal circulation in the atmosphere (Peixoto & Oort 1992). The release and absorption of latent heat due to the freezing and melting of ice may alter the seasonal air temperature cycle and induce local climate. Freezing at the ice bottom rejects salt, increasing the ocean salinity, whereas melting of sea ice will decrease the ocean surface salinity. The ice-ocean interaction can affect the stability of the upper oceans and alter the water circulation throughout the world oceans (e.g. Aagaard & Carmack 1989). In addition, the sea ice cover has major effects on wintertime marine activities in the sub-polar regions by obstructing marine navigation, transportation and oil drilling operations.

The heat exchange between the air and the ice, the heat conduction in ice and snow, the variation of ice thermal properties, the phase changes in ice growth and melt, and the ice-ocean interaction are the main topics of sea ice thermodynamics. In this thesis, we developed a one-dimensional thermodynamic sea ice model and performed various modelling studies in two different regional seas, i.e. in the Bohai Sea and the Baltic Sea.

The Bohai Sea (117.5°-121.1°E, 37.1°-41.9°N) is a mid-latitude sea off the northeast coast of China. The Liaodong Bay in the northern Bohai Sea is normally ice-covered for 3 months in the winter season (Wu & Leppäranta 1988). The Bohai Sea ice has a great impact on coastal and near-shore oil-drilling operations. The Baltic Sea in Northern Europe (17.2°-30.3°E, 56.8°-65.8°N) is located further north than the Bohai Sea. The ice season lasts from a few weeks in the southern Baltic Sea up to more than half a year in the north. The Baltic Sea ice has a self-evident and very disturbing impact on winter navigation.

Cryosphere-Climate Interactions

Fig. 1. The numerous feedback mechanisms and relationship between the cryosphere and the global climate system. Lists in the upper boxes indicate important state variables, while lists in the lower boxes indicate important processes involved in interactions. Arrows indicate direct interactions. Adapted from G. Flato (Online publ: EOS science implementation plan (1999), Chapter 6: Cryospheric Systems (http://eospso.gsfc.nasa.gov/ sci_plan/chapters.html).

Ice research in the Bohai Sea and especially in the Baltic Sea has been carried out for many years. Numerical modelling of the Bohai Sea ice began in 1980's. A dynamic-thermodynamic sea ice model was developed by Wu & Leppäranta (1988) with its main emphasis on ice dynamics. This model has been further developed for ice dynamics research and the Bohai Sea ice operational forecasts (Wu & al. 1997, 1998). The thermodynamic ice process was parameterized in Wang & Wu (1994) and Wang & al. (1999). Numerical modelling of the Baltic Sea ice begun in the early 1970's. Several generations of ice dynamic and thermodynamic models have been developed (e.g. Udin & Ullerstig 1976, Leppäranta 1981, Leppäranta 1983, Omstedt 1990, Leppäranta & Zhang 1992, Omstedt & al. 1994, Omstedt & Nyberg 1995). Sea ice modelling is still developing. Research efforts are being devoted to modelling of the seasonal ice climate (Haapala & Leppäranta 1996, Haapala 2000), ice dynamics investigations (Zhang 2000), and ice thermodynamics and air-ice interaction, as e.g. in Saloranta (2000) and in the various studies of this thesis.

1.2 Objectives and structure of this thesis

The main aims of the study were:

a) To construct a physically-based numerical sea ice model.
b) To investigate the ice surface heat balance and understand the role of surface radiative and turbulent heat fluxes in the ice thermodynamics.
c) To study the turbulent exchange between the air and ice.
d) To model the thermal regimes of ice and snow in seasonally ice-covered seas and to understand the ice physics during thermal equilibrium and the early melting season.
e) To construct a numerical scheme for a sea ice thermodynamic model using the integral interpolation method.
f) To study the effects of the numerical resolution on the results of the ice thermodynamic model.
g) To study the effects of warm air advection on the ice thermodynamics by coupling the ice model with a two-dimensional mesoscale ABL model.

This thesis, consisting of six papers, is composed of the modelling of the ice thermodynamics and the air-ice thermal interaction. The main focus is upon the model physics and the numerical scheme. The main topic of each original article is summarized below.

Paper **I** presented a one-dimensional thermodynamic sea ice model based on the full heat conduction equation. Special attention was paid to the construction of a conservative numerical scheme. The model is the first one of its kind for the Bohai Sea ice.

The further development of the model by detailed consideration of the ice physics and parameterization of the air-ice interaction was presented in paper **II**. The numerical simulations were made against the Bohai Sea and the Baltic Sea field measurements.

Paper **III** and the model simulations presented in section 5.2 of this summary show the outcome of recent Baltic Sea ice modelling. The ice physics during the ice thermal equilibrium and the early melting season was investigated.

In ice growth and melting the boundary conditions are crucial. Papers **IV** and **VI** study the air-ice interaction. Paper **IV** deals with the turbulent heat exchange between air and ice, while in paper **VI** we constructed a coupled mesoscale atmospheric boundary layer (ABL) and sea ice thermodynamic model and applied it in a two-dimensional study.

Numerical integration of the heat conduction equation is an essential part of numerical sea ice thermodynamic models. The dependency of the accuracy of the model results on the resolution of the finite difference scheme was studied in Paper **V**.

The remainder of this summary is organized as follows: the author's contributions to the original articles are described in 1.3. Field data acquired from the Bohai Sea and the Baltic Sea areas are described in section 2. Section 3 gives a general description of thermodynamic sea ice modelling. The mathematical aspects of the ice model are introduced in section 4. Section 5 presents the main results of this thesis. Finally, the conclusions are drawn in section 6.

1.3 The author's contribution

The author of this thesis is fully responsible for papers **I** and **V**, and for this summary. The author is mostly responsible for paper **III**. The author has been responsible for development and implementation of the model and the simulations made in the papers. In paper **II** the author carried the main responsibility for the models' review, field data analysis and the numerical simulations. About half the theoretical model construction was performed by the author. The author's contribution in paper **IV** focused especially on the calculations. In paper **VI** the author was responsible for the model coupling work, simulations and for half of the result analyses.

2 FIELD EXPERIMENTS AND OBSERVED DATA

2.1 The Bohai Sea ice field data

Since the late 1980's, an oil-platform (JZ-20-2-1) located in LiaoDong Bay, in the northern Bohai Sea, has been utilized as an ice observation station during the winter season. The dynamic features of mechanical interaction between sea ice and the platform were the main subjects to be monitored. The ice thickness was difficult to measure since the *in situ* ice field was normally an active drifting area (Fig. 2). The meteorological data were measured continuously by various sensors mounted at a height of about 40 m above the sea surface on a weather mast on the platform. The air temperature (T_a), wind (V_a) and relative humidity (Rh) were recorded. The solar radiation was also measured, but the cloud observations were missing. A period of five days' continuous meteorological measurements was selected from the data set of winter 1990/91 and applied in paper **I** for a trial of the ice model numerical simulation. This test was made primarily in order to validate the model and its numerical scheme.

Fig. 2. A photograph showing the oil-platform (JZ-20-2-1) located in LiaoDong Bay, in the northern Bohai Sea.

Fig. 3. The weather mast of the Finnish-Chinese winter expedition. All the field measurements were made within a radius of 200 m of the mast (Seinä & al. 1991).

A joint Finnish-Chinese winter expedition (1990/91) was carried out in a coastal area (BaYuQuan) in the north part of LiaoDong Bay for a period of two weeks. A weather mast was deployed on the fast ice region, and wind, temperature and relative humidity were measured at heights of 10 m, 4.5 m and 2 m (Fig. 3). The near-surface incoming and reflected solar radiation was also measured. The ice temperatures at various depths were recorded by thermistor strings. The ice thickness was observed manually each day and the ice salinity was determined from ice core samples. The sea current below the ice layer was also measured. The data quality was in general good, but some technical failures occurred during the experiment (Seinä & al. 1991). The experiment was planned in order to better understand the air-ice-sea interaction, to determine the heat exchange coefficients of the atmosphere-ice-water system, and to define various factors of the ice thermodynamic processes. The expedition provided essential weather, ice and ocean data to validate our ice model. Ice modelling studies based on this data set are presented in paper **II**. Table 1 gives a summary of the Bohai Sea ice data employed in this thesis.

Table 1. Summary of the data from the Bohai Sea field experiments in winter 1990/91.

	Platform measurement	BaYuQuan experiment
Time period for the experiment	More than 3 months	25 Jan. – 7 Feb.
Data for ice modelling	7 - 11 Jan. (5 days)	30 Jan. – 7 Feb. (8 days)
Data sampling time interval	10 minutes	1 hour
Location	40.4°N, 121.4°E	40.3°N 122.1°E
Average data for modelling period		
V_a	6 ms^{-1}	4 ms^{-1} (4.5 m height)
T_a	-7 °C	-9 °C (10 m height)
Rh	70 %	68 % [1]
$T_a > 0.0$ °C (portion of data)	0 %	0 %
solar irradiance. (daytime ave.) [2]	31 Wm^{-2} (net)	283 Wm^{-2} (downward)
surface albedo (α)	-	-
Ice thickness (average)	-	38 cm
Snow thickness (average)	-	< 1 cm
Mean water level relative to the ice surface	-	-4 cm

[1] The weather mast measurement failed. The value corresponds to the average of manual observations made once a day.

[2] The small value from the platform measurement is probably due to some fault in the radiative sensors and the unknown cloudiness effect. The measurements of reflected solar radiation suffered technical failures in both experiments

2.2 The Baltic Sea ice field data

Monitoring sea ice in the Baltic Sea has been done in every winter season for many years. Several data sources were utilized in this study. A data bank (IDA) for Baltic Sea ice climate studies was constructed by Haapala & al. (1996). This data bank contains meteorological, oceanographic and hydrographic measurements from around the whole Baltic Sea for 3 individual one-year periods. The data comes from the eight Baltic countries. For the sake of ice modelling research, three Baltic sea ice winters, i.e. 1983/84, 1986/87, and 1991/92, representing respectively normal, severe and mild ice seasons have been chosen as standards. The time interval for the meteorological data samples was 3 hours. The snow and ice thicknesses were measured once a week. We applied IDA data observed at Kemi, a station in the northern Baltic Sea (65.6°N, 24.5°E), for seasonal ice modelling in paper **II** and for the model's numerical resolution study in paper **V**.

The Baltic Air-Sea-Ice Study (BASIS) project of the WCRP-GEWEX-BALTEX program was carried out in 1998-2000. The objective of BASIS was to create and analyse an experimental data set for optimization and verification of coupled atmosphere-ice-ocean models (Launiainen 1999). One field experiment (BASIS-98) organized in winter 1997/98 in the northern Baltic Sea formed the central element of BASIS. The equipment used to gather the data for

ice modelling included a weather mast, a sonic anemometer, radiometers, and an ice thermistor string. The BASIS-98 field data were introduced in papers **III** and **IV**, and these data formed the basis for the thermodynamic sea ice modelling and air-ice coupling studies presented in the papers. Another ice expedition, BASIS-99, was carried out in the following winter; this covered a shorter period of similar field measurements. Some modelling studies using those data are presented in section 5.2 below. For the BASIS experiments, instrument calibrations were made both before and after the measurements. The data were believed to be of better quality than those obtained from the Bohai Sea. The BASIS field experiments are summarized in Table 2.

3 MODELLING SEA ICE THERMODYNAMICS AND AIR-ICE COUPLING

Studies of water ice thermodynamics were already being made in the 1800s. Stefan's law (Stefan 1891), which describes the analytic solution of water ice growth, is regarded as the first reference. This method has been adapted for the first-order prediction of sea ice growth (Simpson 1958, Anderson 1961, Leppäranta 1993). The numerical study of sea

Table 2. Summary of BASIS experiments.

	BASIS-98	BASIS-99
Time period for the expedition	16 Feb. – 7 March	19 Mar. – 26 March
Data for ice modelling	18 days	6 days
Data sampling time interval	10 minutes	10 minutes
Location	63.1°N, 21.2°E	63.9°N, 22.9°E
Average data for modelling period		
V_a (10 m height)	7.6 ms^{-1}	4.7 ms^{-1}
T_a (10 m height)	-4.3 °C	-1.6 °C
Rh (4.5 m height)	78 %	84 %
$T_a > 0.0$ °C (portion of data)	39 %	20 %
solar irradiance (daytime ave.)	139 Wm^{-2} (downward)	188 Wm^{-2} (downward)
mean surface albedo (α)	0.73	0.81
Average ice thickness	38.6 cm	44.6 cm
Snow thickness		
soft snow	-	9 cm
hard snow	-	18 cm
average snow thickness	4.3 cm	23.1 cm
Mean water level relative to the ice surface	-1.4 cm	+7.9 cm

ice thermodynamics began in the 1960s. Early thermodynamic sea ice modelling can be found in the work of Untersteiner (1964), Maykut & Untersteiner (1971), and Semtner (1976). The Maykut & Untersteiner (1971) model has been the basic advanced model for process studies, while the Semtner (1976) model is suitable for climate research.

During the past few decades, several thermodynamic sea ice models have been developed based on these two models (e.g. Gabison 1987, Ebert & Curry 1993, Flato & Brown 1996). Attention was given to different aspects of the thermal response of ice and the air-ice-ocean interactions. For instance, in the Gabison model, the oceanic mixed layer was considered in calculating the ice freezing and break-up. Ebert and Curry derived a complex parameterization of surface albedo to study the radiative feedback between the atmosphere and sea ice. A review of ice thermodynamic modelling is given in paper **II**. The various ice thermodynamic processes have been gradually taken into consideration with more and more detail. Recent modelling work by Bitz & Lipscomb (1999) and Winton (2000) emphasise the importance of the internal melt around brine pockets.

In the work comprising this thesis, a one-dimensional multi-layer thermodynamic sea ice model was created. The main physical processes in the model involve the heat conduction inside the ice and snow, and the heat flux and mass phase change at the ice and snow boundaries. A schematic presentation of the model is given in Fig. 4.

3.1 Thermal processes inside ice and snow

3.1.1 Ice/snow heat conduction

The thermal regime of ice and snow is usually described by a one-dimensional heat conduction equation (e.g. Maykut & Untersteiner 1971)

$$(\rho \cdot c)_{i,s} \frac{\partial T_{i,s}(z,t)}{\partial t} = \frac{\partial}{\partial z}\left(k_{i,s}\frac{\partial T_{i,s}(z,t)}{\partial z}\right) - \frac{\partial q_{i,s}(z,t)}{\partial z} \quad (1)$$

where T is the temperature (Kelvin), ρ is the density, c is the specific heat, k is the thermal conductivity and $q(z,t)$ is the amount of solar radiation that penetrates below the surface layer. The subscripts i and s denote the ice and snow, respectively. In the ice model, the vertical coordinate z is taken as positive downward and t denotes time.

The thermal variation of sea ice depends on its multi-phase constitution (ice crystal, solid salt crystal and liquid brine, inclusion of gases and other impurities). Studies made by Assur (1958), Schwerdtfeger (1963), and Ono (1968) suggested complex expressions for sea ice thermal conductivity and specific heat depending on ice temperature and salinity. The parameterizations of thermal conductivity and heat capacity (density times specific heat) by the temperature and salinity-dependent formulae introduced by Untersteiner (1964) are often used for ice
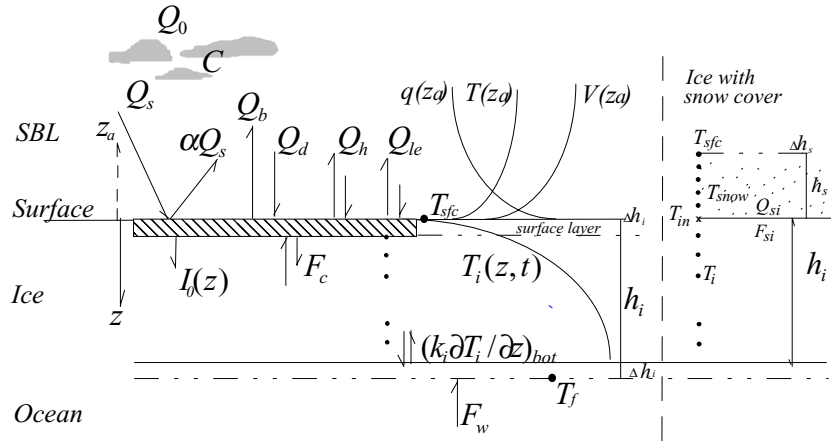
Fig. 4. Structure of the one-dimensional thermodynamic sea ice model (adapted from paper **II**). The vertical dots refer to the spatial grids in the ice and the snow.

modelling studies (e.g. Maykut & Untersteiner 1971, Ebert & Curry 1993):

$$k_i = k_{i0} + \beta s_i / (T_i - 273.15) \tag{2}$$

$$(\rho \cdot c)_i = \rho_0 c_0 + \gamma s_i / (T_i - 273.15)^2 \tag{3}$$

where, k_{i0}, ρ_0 and c_0 are the thermal conductivity, density and specific heat, respectively, of pure ice, s_i is the ice salinity, and β and γ are constants. Such parameterizations are quite sensitive at temperatures near to 0 °C due to the presence of brine. We use these expressions in our model. Since the ice salinity showed small values (< 10 ppt) in the Bohai Sea and the Baltic Sea (Seinä & al. 1991, Weeks & al. 1990, Vihma & al. 1999), we assumed k_i to be less sensitive to s_i by giving it a value of 1.5 Wm^{-1}K^{-1} when T_i approaches 273.15K. This small value was derived from ice temperature profile measurements during a melting period in BASIS-98.

Sea ice salinity (solid salt crystal and liquid brine) distributions are affected by the ice temperature. The variation of this component is described by a conservation equation coupled with Eq. (1) (Cox & Weeks 1988). Since the response time of the variation of salinity is longer than that of the ice temperature, parameterizations of ice salinity as ice-depth dependent (Cox & Weeks 1974, Weeks & Ackley 1986, Kovacs 1996) are usually applied in the ice models. However, those parameterizations may not be valid for low-salinity ice (Kovacs 1996). Accordingly, depth-averaged ice salinity measurements from ice core samples are used in our modelling studies (papers **II**, **III**, and **V**).

The effect of a snow cover on top of the ice is taken into account by solving separately the heat conduction equation in the snow. The snow-ice interface temperature T_{in} is calculated according to the flux continuation assumption $F_{si} = Q_{si}$, where F_{si} and Q_{si} are the conductive heat fluxes at the snow-ice interface. Snowfall is given as forcing data. The snow density is set as a constant, but its value varies, depending on the applications. It is assumed to be 150 kg m^{-3} for newly-fallen snow and 450 kg m^{-3} for wind slab or drift snow. The thermal conductivity of snow is calculated as a function of snow density. The relationship suggested by Yen (1981) is often used in ice models (Ebert & Curry 1993, Saloranta 1998, papers **II** and **III**):

$$k_s = 2.2236(\rho_s / 1000)^{1.885} \tag{4a}$$

A more recent study by Sturm & al. (1997) suggests that the thermal conductivity of seasonal snow can be expressed as:

$$k_s = 10^{(0.002650\rho_s - 1.652)}, \quad \rho s \leq 600 \text{ kgm}^{-3} \tag{4b}$$

This formula is used in paper **VI** and the calculation in section 5.2 below.

3.1.2 Penetrating solar radiation and extinction coefficient

The amount of solar radiation penetrating below the surface depends strongly on its wavelength, the angle of incidence, and the structure of the sea ice. For ice modelling purposes, however, simple parameterizations based on the Bouguer-Lambert law are often used (Untersteiner 1964, Maykut & Untersteiner 1971, Grenfell & Maykut 1977):

$$q_i(z,t) = i_0(1 - \alpha_i)Q_s e^{-\kappa_i(z - \bar{z})} \quad z \geq \bar{z} \tag{5a}$$

where α_i is the surface albedo of ice, Q_s is the incoming short-wave radiation at the surface and $(1 - \alpha_i)Q_s$ expresses the net downward solar radiation at

the surface. The extinction coefficient κ_i is assumed to be 1.5 m^{-1} (Untersteiner 1961) and i_0 is defined as the fraction of the wavelength-integrated incident irradiance transmitted through the top $\bar{z} = 0.1$ m of the ice, and parameterized as a function of sky conditions (cloud fraction, C) and sea ice colour. For example, $i_0 = 0.18(1-C) + 0.35C$ for white ice, and $i_0 = 0.43(1-C) + 0.63C$ for blue ice (Grenfell & Maykut 1977, Perovich 1996).

Near the surface, κ_i can be one or two orders of magnitude larger than 1.5 m^{-1} (Grenfell & Maykut 1977). Within the top 0.1 m in the ice, we assume that radiation follows the relationship

$$q_i(z,t) = (1-\alpha_i)Q_s e^{-\kappa_{i1}z} ,$$
$$\kappa_{i1} = -10 \times \ln(i_0) \qquad 0 < z < \bar{z} \qquad (5b)$$

Hence, the extinction coefficient κ_{i1} is valid for the very uppermost layer is obtained by fitting the values of i_0 of Grenfell & Maykut (1977) observed at a depth of 0.1 m in the ice. For example, $\kappa_{i1} = 17$ m^{-1} for white ice and clear sky conditions. Such a two-layer scheme for $q_i(z,t)$ was used in our model. A two-layer scheme for $q_i(z,t)$ but with a linear profile fitted to the i_0 of Grenfell & Maykut (1977) has been used earlier by Sahlberg (1988).

Alternatively, $q_i(z,t)$ can also be derived from a radiative transfer model (e.g. Grenfell 1979, Brandt & Warren 1993, Liston & al. 1999). In these studies, the wavelength of the irradiance and the structure of the sea ice are taken into account in a more sophisticated manner. A comparison between the $q_i(z,t)$ for blue ice given by (5) and by Liston & al. (1999) with a radiative transfer model is given in paper **V**.

In snow, the penetrating solar radiation in snow is more consistent with the Bouguer-Lambert law, i.e. $q_s(z,t) = (1-\alpha_s)Q_s e^{-\kappa_s z}$, where the extinction coefficient κ_s varies from 5 m^{-1} for dense snow up to almost 10 times larger for newly-fallen snow, depending on the snow density and grain size (Perovich 1996).

3.2 Thermal processes at the boundaries

The thermal regimes of ice and snow are strongly dependent on the external conditions at the boundaries. In our model, a flux boundary condition (of Neumann type, in mathematical terms) is set up at the surface, while at the ice bottom a constant freezing temperature (Dirichlet type) is assumed, and the ice-ocean interaction is solved by a simple mass phase equation.

3.2.1 The surface heat balance

The ice surface heat balance may be written as

$$(1-\alpha)Q_s - I_0 + Q_d - Q_b + Q_h + Q_{le} + F_c = F_m \qquad (6)$$

where I_0 is the solar radiation penetrating below the surface layer. The incoming atmospheric long-wave radiation is Q_d, and Q_b is the long-wave radiation emitted by the surface. The turbulent fluxes of sensible heat and latent heat are Q_h and Q_{le}, respectively. F_c is the surface conductive heat flux and F_m is the heat flux due to surface melting. An inaccuracy in estimating the surface heat flux components may lead to a significant error in the total surface heat balance. The error of each estimated surface flux tends to be smaller than the magnitude of the flux itself, but the net surface heat balance maybe comparable to the error of an individual flux component. Each surface heat flux component therefore needs to be specified carefully in ice models.

Radiative fluxes

The net short-wave and long-wave radiation are often an order of magnitude larger than the other surface heat fluxes and are therefore of primary importance in the energy and mass balance of the ice cover.

The downwelling radiation fluxes are a complicated function of many properties in the atmospheric column. A radiative transfer model would be necessary in order to get the most accurate results. However, the usual limitation of available input data and the excessive computational burden usually dictate the use of simple radiative flux parameterizations in sea ice models (Key & al. 1996).

The simple schemes for downwelling short-wave radiation in clear sky conditions (Q_0) of Lumb (1964), Sellers (1965), Zillman (1972), Moritz (1978), Bennett (1982), and Shine (1984) were derived based on extensive field observations from various areas. That of Zillman (1972) and its adapted alternative by Shine (1984) are often used in ice thermodynamic models (e.g. Parkinson & Washington 1979, Flato & Brown 1996 and studies in this thesis):

$Q_0 (Zillman)$

$$= \frac{S\cos^2 Z}{\left[(\cos Z + 2.7) \times e \times 10^{-3} + 1.085\cos Z + 0.10\right]} \qquad (7a)$$

$Q_0 (Shine)$

$$= \frac{S\cos^2 Z}{\left[(\cos Z + 1.0) \times e \times 10^{-3} + 1.2\cos Z + 0.0455\right]} \qquad (7b)$$

where S is the solar constant, Z is the local solar zenith angle and e is the vapour pressure. For all-sky conditions, the cloud effect is taken into account according to Bennett (1982), i.e., $Q_s = Q_0(1-0.52C)$ and the cloud fraction C is from 0 to 1.

The downwelling long-wave radiation is essentially defined as a function of air temperature: $Q_d = \varepsilon^* \sigma_a T_a^4$, where ε^* is the effective atmospheric emissivity, that is a function of cloudiness and water vapour pressure, and σ_a is the Stefan-Boltzmann constant. Simple schemes for Q_d under clear skies can be found from studies made by Ångström (1918), Brunt (1932), Berljand & Berljand (1952), Kuzmin (1961), Efimova (1961), Swinbank (1963), Marshunova (1966), Idso & Jackson (1969), Maykut & Church (1973), Brustaert (1975), Satterlund (1979), Ohmura (1981), Idso (1981), Andreas & Ackley (1982), Prata (1996) and Guest (1998). We performed a comparison of the selected schemes above in paper **II**. In hard freezing conditions, the results based on the various schemes show a lot of mutual scatter, but generally converge for temperate open ocean conditions. In papers **II**, **III** and **V**, the Q_d were estimated by the scheme of Efimova (1961), while in paper **VI**, the scheme of Prata (1996) was used, i.e.

$$Q_d \, (Efimova)$$
$$= (0.746 + 0.0066 \cdot e) \cdot \sigma_a \cdot T_a^4 \cdot (1 + 0.26C) \qquad (8a)$$

$$Q_d \, (Prata)$$
$$= \left(1 - (1+\eta) \cdot \exp\left\{-\sqrt{1.2 + 3.0 \cdot \eta}\right\}\right) \sigma_a \cdot T_a^4 \cdot (1 + 0.26C) \qquad (8b)$$
where $\eta = 46.5 \times (e/T_a)$

The cloud effect $(1+0.26C)$ used is due to Jacobs (1978). The radiation emitted from an ice or snow surface is given by the Stefan-Boltzmann radiation law $Q_b = \varepsilon \sigma_a T_{sfc}^4$ in which ε is the surface emissivity (0.97), and T_{sfc} is the surface temperature.

The solar radiation penetrating below the surface layer (I_0) is that part of the energy that contributes to the internal heating of the ice/snow. For an ice layer, it is parameterized as a portion (0.17 ~ 0.35) of the total net surface solar radiation $(1-\alpha)Q_s$ depending on sky conditions and the optical properties of the ice (e.g. Grenfell & Maykut 1977). This flux attenuates below the ice surface ($z > 0.1$ m) according to the Bouguer-Lambert law. Such an assumption implicitly indicates that a large portion of solar radiation contributes to the surface heat balance by usually specifying the surface thickness to be more than 0.1 m. In our model, we assumed that the variation of I_0 depends directly on the thickness of the surface layer (see, section 3.1.2 and paper **V**).

The surface albedo depends strongly on the radiation's spectral distribution, surface properties and the sun's altitude. For detailed studies, a complete radiative transfer model would be needed (see the reviews by Perovich, 1996). For thermodynamic ice modelling, Ebert & Curry (1993) developed a parameterization of the surface albedo taking into account the spectral variation and the effect of solar zenith angle on the albedo. The solar spectrum was divided into four intervals and five surface types were included. Such a treatment aims towards a better understanding of the radiative feedbacks between the atmosphere and the sea ice. In our model, the surface albedo is assumed to be a single parameter (bulk value) depending on the surface status (Perovich 1991, 1996). It ranges from 0.85 to 0.77 for dry and wet snow, and from 0.7 to 0.5 for frozen ice and wet ice. For the dirty ice in the Bohai Sea, a value of 0.55 was used.

Conductive heat flux

The conduction of heat at the surface is given by $F_c = k_{i,s} \, (\partial T_{i,s}/\partial z)\big|_{z=sfc}$. During the growth phase, the surface conductive heat flux is upward. During an ice thermal equilibrium phase, a sub-surface temperature maximum can sometimes be generated due to the penetrating solar radiation while the surface may still remain cold. Thus the heat conductive flux may change its direction below the surface. A numerical modelling trial of such phenomena is given in paper **II**. In the melting phase, the ice may reach an isothermal state in the upper layer, indicating a non-conduction case, i.e. $F_c = 0$. The ice and snow may also reach an isothermal state in the upper layer during a cold phase (temperature below freezing point). For example, during warm air advection over an initially cold ice region, the surface heating may gradually give rise to a temperature minimum below the surface. As a consequence, the direction of surface conductive heat flux may reverse, indicating a stage with $F_c = 0$. A detailed study of such phenomena is given in paper **VI**.

Turbulent fluxes and air-ice coupling

The turbulent fluxes of sensible and latent heat are calculated by the bulk formulae:

$$Q_h = -\rho_a c_p C_H (\Theta_{sfc} - \Theta_{za}) V_{za} \qquad (9)$$

$$Q_{le} = -\rho_a L_v C_E (q_{sfc} - q_{za}) V_{za} \qquad (10)$$

where ρ_a is the air density, c_p the specific heat of air, L_v the enthalpy of vaporization, and C_H and C_E are the turbulent transfer coefficients, Θ the potential temperature, V the wind speed, and q the specific humidity. The subscripts *sfc* and *za* refer to the surface and a height of *za* in the air, respectively. The turbulent transfer coefficients are often taken as constants (1.2×10^{-3} - 1.75×10^{-3}) in large scale ice models (e.g. Parkinson & Washington 1979). In our

model, C_H and C_E are estimated based on the Monin-Obukhov similarity theory (Monin & Obukhov 1954, Garratt 1992). Then, the turbulent heat transfer coefficients are defined:

$$C_H = k_0^2 (\ln(za/z_0) - \Psi_M(za/L))^{-1} \cdot \\ (\ln(za/z_T) - \Psi_H(za/L))^{-1} \qquad (11)$$

$$C_E = k_0^2 (\ln(za/z_0) - \Psi_M(za/L))^{-1} \cdot \\ (\ln(za/z_q) - \Psi_E(za/L))^{-1} \qquad (12)$$

where z_0, z_T and z_q are the roughness lengths for the wind speed, air temperature and water vapour, respectively and k_0 is the von Karman constant (0.4). The universal functions Ψ_M, Ψ_H and Ψ_E characterize the effect of the atmospheric surface layer stratification, in which za/L is a dimensionless stability parameter with L the Obukhov length (Obukhov 1946):

$$L = u_*^3 T_0 \rho_a c_p / \left[g k_0 Q_h (1 + 0.61 T_0 c_p E / Q_h) \right] \qquad (13)$$

where u_* is the friction velocity, g the acceleration due to gravity, T_0 a reference temperature and E the turbulent flux of water vapour. We use the universal functions of Holtslag & De Bruin (1988) for the stable region ($za/L \geq 0$), and those of Högström (1988) for the unstable region ($za/L \leq 0$). For the local roughness parameters, whenever the site-specific values are not known, we use for the ice and snow z_0 values from the formula of Banke & al. (1980) and for $z_{T,q}$ the formula of Andreas (1987). The former is based on on-site observed or estimated geometric ice roughness (if assumed as 10 cm it yields $z_0 = 0.001$ m). This provides the aerodynamic roughness of z_0 after which $z_{T,q}$ is deduced from z_0 and u_*.

The calculation of the turbulent fluxes is iterative, since L depends on the fluxes (e.g. Launiainen & Vihma, 1990). However, L can be related to the bulk Richardson number using the flux-profile relationships (e.g. Launiainen 1995). The bulk Richardson number is calculated directly from aerodynamic observations; the flux calculation can then be non-iterative. Such a procedure (Launiainen & Cheng 1995) was used in the ice model. Numerical tests indicated that the results yielded by the iterative and non-iterative algorithms are quite close to each other. The dimensionless profile gradients of wind, temperature and specific humidity can be given in terms of the Monin-Obukhov similarity theory. Since the stability parameter, fluxes and scaling parameters are solved simultaneously with the ice model conductivity equation, the profiles of wind, temperature and moisture in the atmospheric surface layer can be obtained as well.

In addition to the bulk formulae, the turbulent surface fluxes can be expressed in their gradient forms, e.g.

$$\tau = \rho_a u_*^2 = \rho_a K_M \frac{\partial V}{\partial z_a} = \rho_a \frac{k_0 u_* za}{\Phi_M(za/L)} \frac{\partial V}{\partial z_a} \qquad (14)$$

$$H = -\rho_a c_p K_H \frac{\partial \Theta}{\partial z_a} = -\rho_a c_p \frac{k_0 u_* za}{\Phi_H(za/L)} \frac{\partial \Theta}{\partial z_a} \qquad (15)$$

where τ is the momentum flux. The eddy diffusivities for momentum K_M and heat K_H are parameterized as functions of the universal functions in the gradient forms (Φ_M and Φ_H). The turbulent fluxes estimated by such a gradient method were presented in paper **IV** and the results were compared with the eddy-flux measurements and with the calculations from the ice model.

Evolution of upper boundary

The ice layer has a moving boundary on both sides due to phase changes. If the surface temperature calculated from (6) tends to become higher than the melting point (T_m), it is kept at that value, and the excess energy is used to melt the ice. The surface heat balance (6) then becomes

$$(1-\alpha)Q_s - I_0 + Q_d - Q_b(T_m) + Q_h(T_m) + Q_{le}(T_m) + F_c(T_m) \\ = \rho_{i,s}(L_f)_{i,s} dh_{i,s}/dt \qquad (16)$$

where (L_f) is the latent heat of fusion and h is the thickness of ice or snow and the flux-terms in brackets are surface temperature ($T_{sfc} = T_m$) dependent. For sea ice $T_m = -0.054 s_i$, depending on ice salinity, while for snow $T_m = 0$. A major concern arises here about to the value of the latent heat of fusion. Theoretically, it is a function of ice salinity and temperature. For salty ice near the melting temperature, $(L_f)_i$ has much smaller values than that for pure ice (Yen 1981). Björk (1992), Bitz & Lipscomb (1999) and Winton (2000) emphases the importance of considering the influence of salinity and temperature on $(L_f)_i$. In our model, we use $(L_f)_s = 334$ kJ kg^{-1}, and $(L_f)_i \approx 0.9(L_f)_s$ following Maykut & Untersteiner (1971) and Ebert & Curry (1993).

During the polar spring and summer, the solar radiation penetrating into snow and ice may become large enough to cause internal melting. This phenomenon has been reported especially for the Arctic and Antarctic ice region (Schlatter 1972, Brandt & Warren 1993, Bøggild & al. 1995, Koh & Jordan 1995, Winther & al. 1996, Liston & al. 1999). Paper **II** presents a theoretical example of modelled sub-surface melting. An attempt at a quantitative calculation of sub-surface melting is given in section 5.2.

3.2.2 Ice-ocean interaction

At the ice bottom, the boundary condition is:

$$T_{bot} = T_f \qquad (17a)$$

$$-(k_i \partial T_i / \partial z)_{bot} + F_w = -\rho_i (L_f)_i \, dh_i / dt \qquad (17b)$$

where T_{bot} is the ice bottom temperature remaining at the freezing point T_f. A typical value of -1.8 °C is often assumed for the freezing temperature of polar sea ice, whereas for the northern Baltic Sea, due to the low salinity, T_f is assumed as -0.26 °C; This is used in paper **III**. In (17b) the term $k_i(\partial T_i/\partial z)|_{bot}$ is the conductive heat flux at the ice bottom, and F_w is the oceanic heat flux.

The oceanic heat flux is a key component in the sea ice energy and mass balance. However, in sea ice thermodynamic models it is often assumed constant (Maykut & Untersteiner 1971, Bitz & Lipscomb 1999). The seasonal variation of F_w is large, especially in the polar ice-covered regions (e.g. Maykut & McPhee 1995, Heil & al. 1996, McPhee & al. 1996). Its proper determination may necessitate coupling to an ocean model (Lemke 1987, Omstedt & Wettlaufer 1992). The sensitivity of the ice to the magnitude of F_w and the dependence of ice-ocean models on the correct specification of F_w make it an effective tuning parameter in model studies (Wettlaufer & al. 1990).

Direct measurements of F_w below the ice layer in the Bohai Sea are not available. A value of 5 Wm^{-2} was assumed and used for the Bohai sea ice modelling in paper **II**. Eddy flux measurements below the sea ice were carried out during the BASIS-98 winter expedition. The average F_w sampling interval was 15-20 minutes. The time series indicated values varying between ± 20 and ± 40 Wm^{-2} at depths of 0.5 and 5 m below the ice surface, respectively (Shirasawa & al. 2001). Taking a time average of the entire BASIS-98 period yields $F_w \approx 1$ Wm^{-2}. This small value was applied in papers **III** and **V**. The oceanic heat flux can be estimated from measurements of ice thickness and ice temperature (Wettlaufer & al. 1990). A sensitivity study based on this procedure was presented in paper **III**. For seasonal ice modelling, adjustments in the value of F_w should be made when significant heat exchange occurs below the ice cover, at least at the beginning of the ice growth season. The study of F_w in our model should be further developed.

3.3 Summary of the ice model used in this thesis

The core of our one-dimensional thermodynamic sea ice model is the ice/snow heat conduction equation

(1) associated with the moving boundary conditions of (6), and (17). Equation (6) can be seen as a polynomial of the surface temperature. This complicated flux boundary is not used directly in the numerical scheme of (1). Instead, we solved the surface temperature from (6) and used it as an upper boundary condition. The model parameters are given in Table 3.

This ice model was originally designed for process studies (papers **I**, **II**, **III**, **IV**). It can be extended for use in polar sea ice thermodynamic modelling once the model parameters are adjusted. This model has already been applied in a study of the surface heat balance in the Weddell Sea (Vihma & al. 2002).

3.4 Coupled mesoscale atmospheric and sea ice thermodynamic model

A coupled atmospheric-ice model was developed in paper **VI** to study the effect of warm-air advection on sea ice thermodynamics. A few studies have been published about warm-air advection over sea ice (e.g. Andreas & al. 1984, Bennett & Hunkins 1986, Kantha & Mellor 1989, Brümmer & al. 1994, Vihma & Brümmer 2002), but they have dealt more with the processes in the ABL. On the other hand, among the numerous studies on sea ice thermodynamics, the air-ice interaction has mostly been taken into account one-dimensionally via the radiative and turbulent exchange (Ebert & Curry 1993, Liston & al. 1999 and paper **II**). We have not found any paper with a special emphasis on the spatial variations due to warm-air advection.

The atmosphere model is a two-dimensional mesoscale atmospheric boundary-layer (ABL) model. In the ABL, the flow is forced by a large-scale pressure gradient. The horizontal momentum equations, the hydrostatic equation, the equation of state, the continuity equation, and the conservation equations for heat and moisture compose the core of the ABL model. The model has (x, σ) coordinates (σ is the atmospheric pressure divided by its surface value). The governing equations for horizontal air motion and heat conservation are as follows:

$$\frac{\partial u}{\partial t} = -u \frac{\partial u}{\partial x} - \frac{d\sigma}{dt} \frac{\partial u}{\partial \sigma} + f(v - v_g) - RT / (p_* + p_t / \sigma) \frac{\partial p_*}{\partial x}$$

$$-\frac{\partial \phi}{\partial x} + \frac{g^2}{p_*^2} \frac{\partial}{\partial \sigma} \left(\rho_a^2 K_{za} \frac{\partial u}{\partial \sigma} \right) \qquad (18)$$

$$\frac{\partial v}{\partial t} = -u \frac{\partial v}{\partial x} - \frac{d\sigma}{dt} \frac{\partial v}{\partial \sigma} - f(u - u_g)$$

$$+\frac{g^2}{p_*^2} \frac{\partial}{\partial \sigma} \left(\rho_a^2 K_{za} \frac{\partial v}{\partial \sigma} \right) \qquad (19)$$

$$\frac{\partial \Theta}{\partial t} = -u\frac{\partial \Theta}{\partial x} - \frac{d\sigma}{dt}\frac{\partial \Theta}{\partial \sigma} + \frac{g^2}{p_*^2}\frac{\partial}{\partial \sigma}\left(\rho_a^2 K_{za}\frac{\partial \Theta}{\partial \sigma}\right) + C_0 \quad (20)$$

where u and v are the horizontal wind components in which u indicates the direction along the model x-axis. Θ is the air potential temperature, T is the air temperature, R is the gas constant, ϕ is the geopotential, $p_* = p_s - p_t$, in which p_s is the surface pressure and p_t is the pressure at the model top (3 km). The factor f is the Coriolis parameter, g is the acceleration due to gravity and C_0 in (20) denotes the temperature change due to the release of condensation heat. The terms with K_{za} in them (18 - 20) are the expressions for the change of momentum and potential temperature due to vertical diffusion. They are given following the K-theory. Turbulence is described by a first-order closure with the vertical (z_a is positive upward in the ABL model) diffusion coefficient $K_{za} = l^2 (dU/dz_a)f(Ri)$, where the mixing length is given by $l = k_0 z_a/(1 + k_0 z_a/\varepsilon_0)$. Here, dU/dz_a is the wind shear, $\varepsilon_0 = 20$ m, and $f(Ri)$ is an empirical function depending on the Richardson number (Ri). In stable stratification conditions, which prevail during warm-air advection over sea ice, $f(Ri) = $ max

[0.02, (1-7Ri)] is used for momentum, heat and moisture. Vertical diffusion is solved by an implicit method, and instead of explicit horizontal diffusion, a weak low-pass filter is applied to all fields. The details of the model's dry dynamics are described in Alestalo & Savijärvi (1985), and the physical parameterizations in Savijärvi (1997). We adjusted the parameter values in our study and used 92 horizontal grid-points and 50 layers with a quasi-logarithmic spacing in the vertical. The model top is at 3 km, where the wind becomes geostrophic. The model grid length is 4 km with flat topography. The structure of the coupled model is shown in Fig. 5. The ice model is coupled with the ABL model at each horizontal grid point. The surface temperature T_{sfc} acts as the key element in the coupling. At each time step, the surface heat fluxes and surface temperature are solved from (6) to (12). The ABL equations are then solved using T_{sfc} as a boundary condition, and the resulting wind speed, air temperature and relative humidity at the lowest level of the ABL model are used as forcing input for the ice model. The surface heat balance and ice thermal regimes are then solved from the ice model.

Table 3. The ice model's parameters. Parentheses denote a standard value. A range of values means that they are case-dependent.

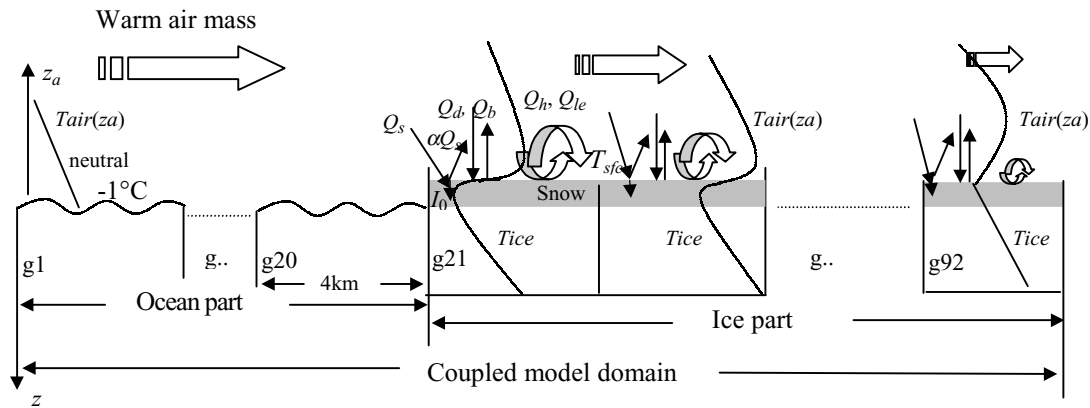|		
Aerodynamic roughness, z_0	(10^{-4} m)	Assumed
Density of air (ρ_a)	1.26 kgm^{-3}	349/T_a
Density of snow (ρ_s)	150 ~ 450 kg m^{-3}	Snow age dependent
Density of sea ice (ρ_i)	(910 kg m^{-3})	
Extinction coefficient of sea ice (κ_i)	1.5 ~ 17 m^{-1}	After Maykut & Grenfell (1977)
Extinction coefficient of snow (κ_s)	15 ~ 25 m^{-1}	Perovich (1996)
Freezing temperature (T_f)	(-0.2 ~ -1.8 °C)	$T_f \approx -0.054 \cdot s_w$, salinity dependent
Heat conductivity of ice (k_{i0})	(2.03 W m^{-1} K^{-1})	Pure ice
Latent heat of fusion ($L_f)_s$	0.33×10^6 J kg^{-1}	Fresh water
Latent heat of fusion of sea ice ($L_f)_i$	0.9×($L_f)_s$	After Maykut & Untersteiner (1971)
Oceanic heat flux (F_w)	(1 ~ 5 W m^{-2})	Assumed
Sea ice salinity (s_i)	0.5 ~10 ppt	Observed in the Baltic Sea and the Bohai Sea
Sea water salinity (s_w)	< 5 ppt	Observed near ice bottom during BASIS-98
Specific heat of air (c_p)	(1004 J kg^{-1} K^{-1})	
Specific heat of ice (c_0)	(2093 J kg^{-1} K^{-1})	Pure ice
Surface albedo of ice (α_i)	(0.7)	0.55 for the dirty ice (Perovich 1991)
Surface albedo of snow (α_s)	(0.8)	> 0.8 for fresh snow (Perovich 1996)
Stefan-Boltzmann constant, σ_a	5.68x10^{-8} Wm^{-2} K	
Surface emissivity (ε)	(0.97)	Assumed
Solar constant (S)	(1367 Wm^{-2})	
von-Karman constant (k_0)	(0.4)	
Constant (β)	0.117Wm^{-1}ppt^{-1}	
Constant (γ)	17.2 ×10^6 JKm^{-3}ppt^{-1}	
Time step of model (τ_t)	600 s ~ 6 hours	
Number of layers in the ice (N_i)	≥ 3 ; 10 ~ 30	
Number of layers in the snow (N_s)	≥ 3; 5 ~ 10	

Fig. 5. Structure of the coupled ABL – sea ice model. The first 20 grid cells (g1–g20) from the inflow boundary represent the open sea with a fixed surface temperature and a fixed inflow temperature profile ($\partial T/\partial z_a$ = -6.5 K km^{-1}). The rest of the grid cells (g21-g92) represent sea ice with a snow cover. (adapted from paper **VI**).

4 NUMERICAL SCHEME OF THE THERMODYNAMIC SEA ICE MODEL

The numerical integration of the heat conduction equation is a main component in a thermodynamic sea ice model. One has to define model resolution (grid sizes and time step) before applying any numerical schemes. For process study a fine resolution scheme is preferred, whereas for ice climatic modelling studies a coarse resolution scheme is often used. Various finite difference schemes have accordingly been applied to Eq. (1). For example, a stable alternating direction explicit method (e.g. Larkin 1964) was applied by Maykut & Untersteiner (1971). The implicit absolutely stable Crank-Nicholson (CN) scheme was used by Gabison (1987), Flato & Brown (1996) and Saloranta (2000) since it has smaller (second order) truncation errors in both the temporal and spatial scales. The simple forward-difference scheme and explicit absolutely stable Dufort-Frankel algorithms are utilized respectively by Semtner (1976) and Ebert & Curry (1993).

A finite difference scheme for a parabolic equation can be derived straightforwardly by replacing the derivative terms with difference quotients. This is a good approximation. However, one may use an approximation of numerical integration, which is sometimes called the integral interpolation method, to derive a scheme. Such a derivation retains the conservative characteristics of the parabolic equation (Li & Feng 1980). This method was implemented to derive the CN numerical scheme of our ice model in paper **I**. An example of how to apply such a method is given in the Appendix of this summary.

The initial condition of the numerical scheme (in-ice/snow temperatures) must be specified. It may arbitrarily depend on the time-scale of the application. For example, an isothermal vertical temperature or a linear interpolation profile between the air temperature and the ice bottom freezing temperature

may be suitable for seasonal ice modelling. For short-time model runs and air-ice coupling, an initialization procedure may be necessary (papers **III** and **VI**). The boundary conditions have been discussed in section 3.2.

The time step of our model varies from 10 minutes (e.g. papers **I**, **III**, **V**) up to hours (paper **II**) depending on the applications. The model grid size is usually in centimetres. One may use a model grid system either with a fixed number of grid points (Lagrangian grid) or one that maintains a constant inner grid size (Eulerian grid). The Lagrangian grid is often used (Semtner 1976, Ebery & Curry 1993, Schramm & al. 1997 and this model). The ice layer has a moving boundary due to the freezing and melting. In order to adapt to the moving grid points, Semtner (1976) used a linear interpolation of in-ice temperature from the previous coordinate to the current one, at each time step, based on the conservation of the total heat content of the ice. However, the effect of salinity and temperature on the specific heat of sea ice was ignored. A procedure assuming the conservation of enthalpy was used by Schramm & al. (1997) to calculate the interior ice temperature taking into account the shift in the grid size, while the volumetric heat capacity was given as a function of ice salinity and temperature. We applied an iterative procedure with a piecewise interpolation to calculate the in-ice temperature at the model grid points at each time step using the values at points given by the previous step. Numerical tests indicated convergence of the result within three steps. A mathematical treatment of the moving boundary of an ice model is given in the technical report of the model (Cheng & Launiainen 1998).

In general mathematical terms, increasing the resolution of a numerical scheme should yield better accuracy of the results and vice-versa. The impact of numerical resolutions on model predictions was studied in paper **V**.

5 RESULTS AND DISCUSSION

5.1 Model validation

Model validations are performed in paper **II**. For a short-term simulation, the modelled ice thickness and temperature are compared with the Bohai Sea ice field measurements. Table 4 gives the observed and modelled ice thickness and temperatures. The data sampling time interval is one day for the ice thickness and one hour for the ice temperature. A model run was made over a total of 210 hours.

The results indicated quite a good accuracy for the model simulations. The larger disagreement in ice temperature in the uppermost layer may be due to the effect of mild weather conditions on the sea ice thermal properties before the start of the model simulation. Such external conditions usually influence ice thermal properties with a time lag. On the other hand, the contamination of on-site surface skin temperature measurements due to dust was an error source in the field data (Seinä & al. 1991).

Pronounced clear-sky weather conditions dominate most of the winter season in the Bohai Sea. The ice temperature showed a clear diurnal cycle due to the short-wave radiation effects, and this was well simulated by the ice model. Figure 6 shows the modelled vertical temperature profiles in air and ice on a cold and on a mild day during the Bohai Sea ice experiment. The sub-surface heating by solar radiation absorption during daytime below the surface is modelled well. During the early morning, the modelled surface-layer inversion is the result of radiative cooling, while during the daytime it is then the effect of warm air because of the mild weather. In this Fig-

ure, the near surface unstable stratification temperature profiles may be explained by the effect of incoming long-wave radiation due to the present of cloud cover. On the other hand, in an interpretation of the surface layer inversion and the results in Figure 6 we have to keep in mind that the atmospheric driving force, especially the air temperature, varies during the experiment and that the case is not purely "one dimensional" in that sense.

The thermally-induced variation of fast-ice thickness at the station of Kemi in the northern Baltic Sea was simulated and compared with measurements. For such seasonal ice evolution, the model was run using historical climatic weather forcing data from the IDA data bank. The model simulations are made for three separate winter seasons. The simulations started from the freezing date of each winter with a 0.05 m initial ice thickness. The ice was considered as having melted when the simulated ice thickness was less than 0.01 m. The errors of modelled and observed ice thickness are given in Table 5.

The results are good, indicating that the model essentially catches the seasonal thermodynamic sea ice variations. Numerical simulation of ice thickness for those three winters was also performed by Haapala & Leppäranta (1996) using a coupled ice-ocean model, and by Saloranta (1998) using a thermodynamic snow/ice model. By comparison with those studies, our results showed a better accuracy of modelled ice thickness during the spring melting season. This may be due to a good parameterization of the air-ice interaction, and an advantageous treatment of the solar radiation penetrating below the surface.

Table 4. Observed and calculated ice thickness and temperature for the Bohai Sea ice study.
(r.m.s = root mean square)

Ice thickness h_i (cm) and Ice temperature T_i (°C)	Average value		Range		(r.m.s.) error
	Obs.	Calc.	Obs.	Calc.	
h_i	38.4	38.8	[33.0 42.3]	[33.0 41.7]	1.0
T_i ---- 6 cm	-6.7	-8.3	[-12.7 -1.8]	[-14.2 -1.8]	2.0
T_i ---- 16 cm	-5.6	-6.2	[-10.5 -1.9]	[-9.9 -2.3]	1.0
T_i ---- 21 cm	-4.8	-5.2	[-7.6 -2.6]	[-7.9 -2.4]	0.9
T_i ---- 31 cm	-2.9	-3.1	[-3.7 -1.5]	[-4.1 -2.0]	0.6

Table 5. Observed and modelled seasonal ice thickness for the Baltic Sea ice study.

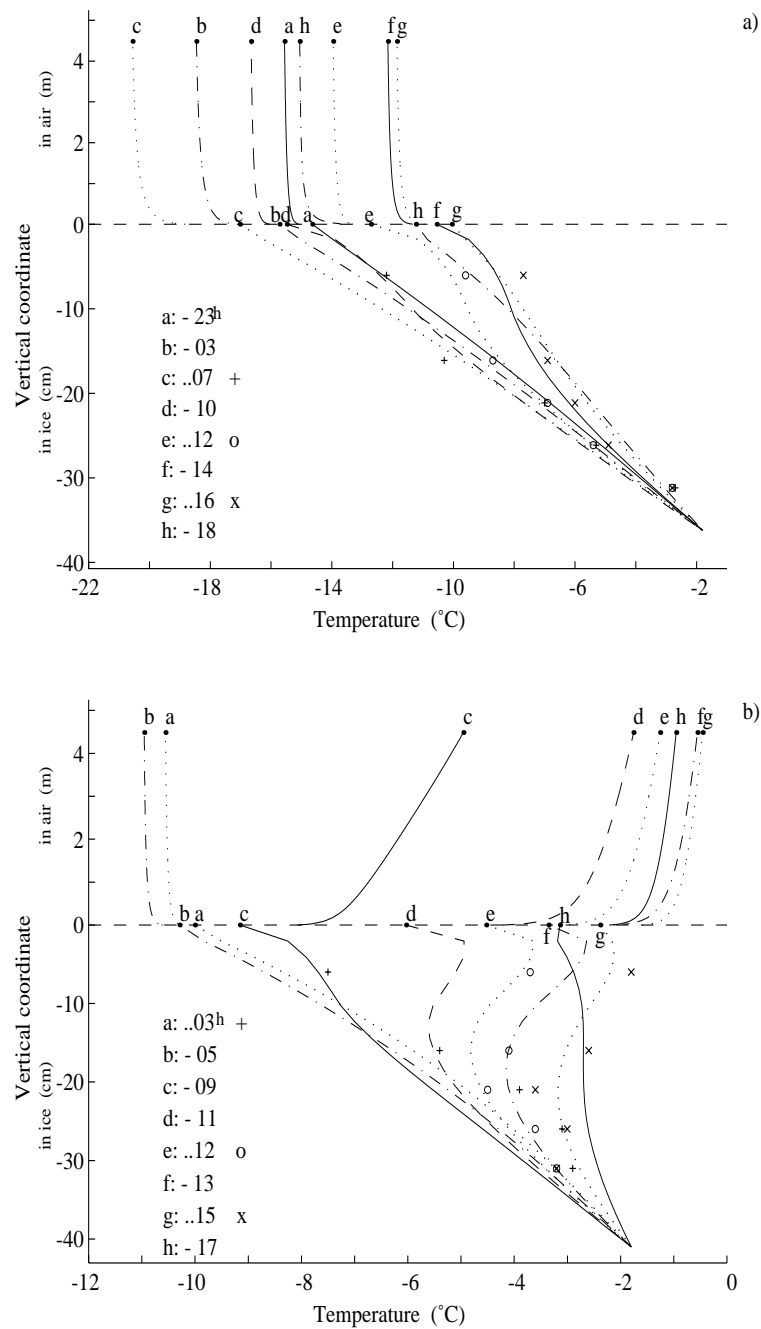| Ice winter	Average value (m)		Mean error (m)	(r.m.s.) error (m)	Covariance (m)	Correlation coefficient
	Obs.	Calc.				
83/84	0.52	0.56	0.04	0.1	0.02	0.88
86/87	0.68	0.72	0.04	0.09	0.06	0.82
91/92	0.34	0.36	0.02	0.05	0.02	0.87

Fig. 6. Vertical air and in-ice temperature profiles. a) during a cold day, from 2300h on 30 Jan. to 1800h on 31 Jan. 1990, from 2300h to 1800h and (b) during a milder day, 5 Feb. 1990, from 0300h to 1700h. A few observations are given (+, o, x) for comparison (note the different vertical scaling in ice and air; redrawn from paper **II**).

A thin layer of new snow may have an active effect on accelerating melting in the spring. This has the opposite effect to that of a snowfall in wintertime, when snow is normally considered as a good insulator and reflects more radiation due to its high surface albedo. New snowfall has a high volumetric extinction coefficient, which can cause a rapid melting on a spring day. The melting of the new snow decreases the surface albedo drastically through the action of the melting water and then provides more short-wave radiation that is available for melting. A hypothetical example was modelled

to demonstrate this effect. As the result, a 3 cm night-time fall of new snow already began to melt in the morning with the diurnal variation of solar radiation occurring at 60° N latitude on April 1st (see, Fig. 11 in paper **II**).

5.2 Superimposed ice freezing and sub-surface ice melting

The thermal variations of sea ice were studied during BASIS-98 and BASIS-99. During the thermal equilibrium stage of BASIS-98, the ice showed little mass phase variations at the ice-water interface. In contrast to the 'quiet' ice bottom, the surface indicated large variability due to snowfall, snowdrift and melting. Observations indicated a snow-to-ice transformation at the snow-ice interface. Numerical modelling suggested that the re-freezing of the surface melt water was a primarily source for snow-ice formation (paper **III**). In the following, we present some new ice model simulations applied to the BASIS field data.

Snow present on top of the ice layer may be partly transformed to snow-ice. This may take place via two different physical processes:

(a) flooded ocean water between the snow and ice forms a slush layer that refreezes over the original ice cover;

(b) melted surface and sub-surface snow water or wet snowfall and rainfall percolates down and refreezes on top of the original ice cover.

Here, we will refer to case (b) as superimposed ice formation.

In the Baltic Sea, incoming snowfall accounted on average for 25-45 mm equivalent water per month from December to February (Kolkki 1969) and snow-ice may contribute to some 1/3 of the total ice thickness (Leppäranta & Seinä 1982). A recent measurement made in the Gulf of Finland in winter 1998/99 indicated that even as much as 43-55 % of the total coastal land-fast ice was snow-ice (Kawamura & al. 2001). The first attempt to model snow-ice formation in the Baltic Sea was made by Leppäranta (1983), while Saloranta (2000) performed a more recent modelling study of the evolution of snow-ice formation. The former paid attention to the ice growth season, while the latter focused on a longer time-scale, i.e. the seasonal snow-ice evolution. The main mechanism for snow-ice formation in their work was (a). Here we study the effect of (b) on snow-ice formation. We pay attention to water through surface and sub-surface melting and its refreezing, while wet-snow and rainfall is not considered. The primary motivation of this work is to quantitatively understand the importance of the superimposed ice formation on sea ice thermodynam-

ics. Such a topic does not seem to have been discussed. The model simulations are carried out with BASIS-98 and BASIS-99 field data.

In order to study superimposed ice formation, we first need to estimate how much melting can be supplied.

i) For a surface layer with its temperature above the melting point, the melting is calculated by (16).

ii) Sub-surface melting occurred mainly due to the effect of absorbed short-wave radiation below the surface. When the ice temperature for a sub-surface layer tends towards a value above the melting point, it is maintained at the melting point; the heat flux balance between this isothermal sub-surface layer and the adjacent upper and lower snow/ice will then be used for the melting calculation. This procedure satisfies the continuity of conductive heat flux in snow/ice and the conservation of energy.

The BASIS-98 field measurements indicated some 39 % of the data with the air temperature above freezing. The model run in paper **III** indeed produced a total surface melting of 12 cm snow. Taking into account the sub-surface melting ii), the re-run model produces about 0.5 cm (4 %) more melting- not a large difference. During BASIS-98, the surface melting mostly occurred when the air temperature was higher than the freezing point. On the other hand, downward solar radiation in February is still quite limited and not strong enough to generate large amounts of sub-surface melting. In BASIS-99, only 20 % of the data had an air temperature above freezing (Table 2). However, the observed daytime average solar radiation was 35 % larger than that in BASIS-98. It was already early spring and sub-surface melting could start.

The model simulation of BASIS-99 was analogous to that presented in paper **III**, i.e., the external forcing was based on the weather mast measurements, and the model parameters were largely based on the field measurements. Ice salinity was from 0.38 to 0.65 ppt. The freezing temperature at the ice bottom was -0.2 °C. According to *in situ* measurements (M. Lundin, pers. comm.), the snow was essentially divided into two layers representing newly-fallen soft snow on top of a wind-slab of hard old snow (Table 2). The average snow densities were 150 kg m^{-3} and 380 kg m^{-3}, respectively. According to Sturm & al. (1997), this suggested that the thermal conductivities were 0.056 and 0.23 Wm^{-1}K^{-1}, respectively. We further assumed the snow extinction coefficient to be 25 m^{-1} and 15 m^{-1} for the upper and lower layer, respectively, following Perovich (1996). Values for the solar radiation and surface albedo were directly taken from the observations. Figure 7 displays the modelled total surface snow melting. The model result indicated a total 4.5 cm melting of which about 20 % was accounted for by the sub-surface melting.
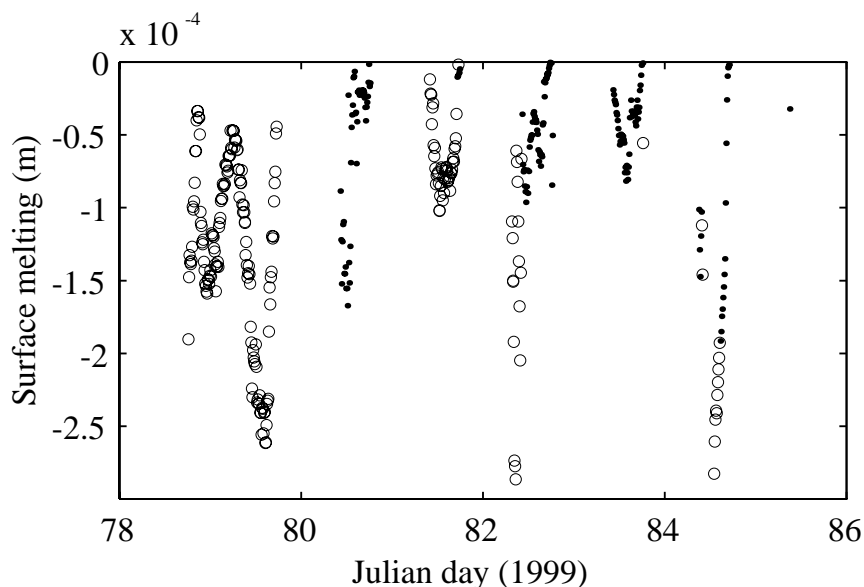
Fig. 7. Modelled snow melting. The circles are the surface melting while dots are the calculated sub-surface melting. The melting value corresponds to a time step of 10 minutes.

Table 6. Sensitivities of surface melting to snow properties. The melting is denoted as a decrease in the snow thickness (cm).

	κ_s (m^{-1})		ρ_s (kgm^{-3})		k_s (Wm^{-1}K^{-1})		Total melting (cm)	Sub-surface melting (cm)
Control Run	soft	dense	soft	dense	soft	dense		
(2 snow layers)	25	15	150	380	0.056	0.23	4.5	0.9 (20 %)
Trail 1	25		380		0.23		3.7	0.5 (13 %)
Trail 2	15		380		0.23		4.0	1.1 (28 %)
Trail 3	25		150		0.056		5.3	1.3 (24 %)
Trail 4	15		150		0.056		5.8	2.3 (40 %)

Some sensitivity tests were carried out in order to see the effect of snow properties on melting. For simplicity, the snow is assumed to be a single layer for each model test and a change is made in a single model parameter. In Table 6 the results are compared with the control run. It can be seen that the sub-surface melting is sensitive to the snow's extinction coefficient while the total surface melting is sensitive to the snow's thermal properties. Such conclusions support the earlier studies of increased sub-surface temperature and sub-surface melting made by Koh & Jordan (1995) who applied a high-resolution frequency-modulated continuous wave radar to detect the onset of sub-surface melting.

We have to emphasise that our sensitivity tests were confined to detecting the effect on sub-surface melting of changing only one parameter at a time. The results of such tests cannot be offered as the final truth. In reality, interaction among all the parameters is expected: this can enhance the effect on both melt-layer thickness and sub-surface temperatures (Bøggild & al. 1995). Modelling of increased sub-surface temperature and sub-surface melting by taking into account such complex interactions among all parameters has not been carried out so far.

The superimposed ice is formed by refreezing of melting water. Assuming the surface melting water is totally refrozen, the modelled ice thickness is in good agreement with the field observations (Fig. 8d in paper **III**). Such an assumption is suitable for the BASIS-98 ice modelling is suitable. The modelled average conductive heat flux in snow was about 19 Wm^{-2} upward. If we neglect the salinity effect on the latent heat of fusion, such a heat flux can produced roughly 0.6 cm of frozen ice per day. In other words, the total 12.5 cm surface melting snow would take about 9 days to completely refreeze. During the melting phase, the snow surface was relatively warm and a downward heat flux in the snow layer was both modelled and measured, indicating that a slush layer may exist for some time. On the other hand, the observed average heat flux in the ice was 8.1 Wm^{-2} and upwards. This is consistent with the same direction of average heat flux in the snow, which means that the slush layer between the snow and the ice was refrozen within the time-scale of the whole expedition.

During BASIS-99, however, the weather conditions were quite mild and not favourable for superimposed freezing. Instead, the percolated melting water may have formed a slush layer above the original ice layer. The observed and modelled snow and ice temperature fields are given in Figure 8. Both measurement and calculation indicated quite a high sub-surface temperature. Unfortunately, the uppermost thermistor recorded an unrealistically high snow temperature and thus is not shown here. Radiative heating of the uppermost sensors in snow or ice on clear days can lead to an incorrect temperature measurement (Brandt & Warren 1993).

Results showed that the sub-surface melting was located within a layer centred about 10 cm below the surface. The model results clearly showed the diurnal variation of snow temperature, while the measurements did not, except for the first day after deployment of the thermistor stick. This maybe due to the effect of the wetness of the snow layer. From the second day of the expedition onwards, the snowfall was seen occasionally mixed with rainfall. The rainfall together with the surface melt water may temporarily fill the porosity of the snow layer before they percolate down to the snow-ice interface, forming the slush layer. In addition, due to a heavy load of snow, the saline water from the ocean may seep up to the snow-ice interface. The latent heat of the water fraction in snow can damp the daily variation in temperature of the snow layer. These effects were, however, not taken into account in the model. Further studies of these effects on superimposed ice formation are needed.

The model results of an increased sub-surface temperature effect have been difficult to verify experimentally, due to the problems involved in measuring the temperature profile using thermal sensors embedded in the snow/ice (Koh & Jordan 1995). To verify such modelling results, more work, both on theoretical considerations and on field observations, is needed.

5.3 Effect of model numerical resolution

In paper **V**, analytical solutions were obtained for the simplified ice model cases. These solutions were then compared to the numerical approximations obtained at various model resolutions. Three simplified model cases which can yield analytical solutions are defined: 1) the Stefan ice growth model; 2) a parabolic diffusion equation with prescribed boundary conditions of the Dirichlet and Neumann types; 3) steady state of 2).

In case 1), the ice model yields quite a good consistency with Stefan's ice growth under various spatial resolutions. This procedure can be used for verification of the numerical scheme. On increasing the model time step (coarser temporal resolution), those model runs with a high spatial resolution showed an oscillation of the ice growth rate. Such numerical perturbations can be attenuated by adopting the numerical scheme in its fully-implicit form. Case 2) showed that the modelled ice temperature approaches the analytical solution by increasing the spatial resolution for both Dirichlet and Neumann boundaries, and the ice temperature differences between the numerical result and the analytical solution decrease exponentially. Case 3 illustrated the asymptotic state in which the solar radiation tends to drive the temperature profile. In such a condition, a high resolution is needed for the numerical model in order to approach the analytical solution closely, especially for the Neumann boundary. The details of these three cases are given in paper **V**.
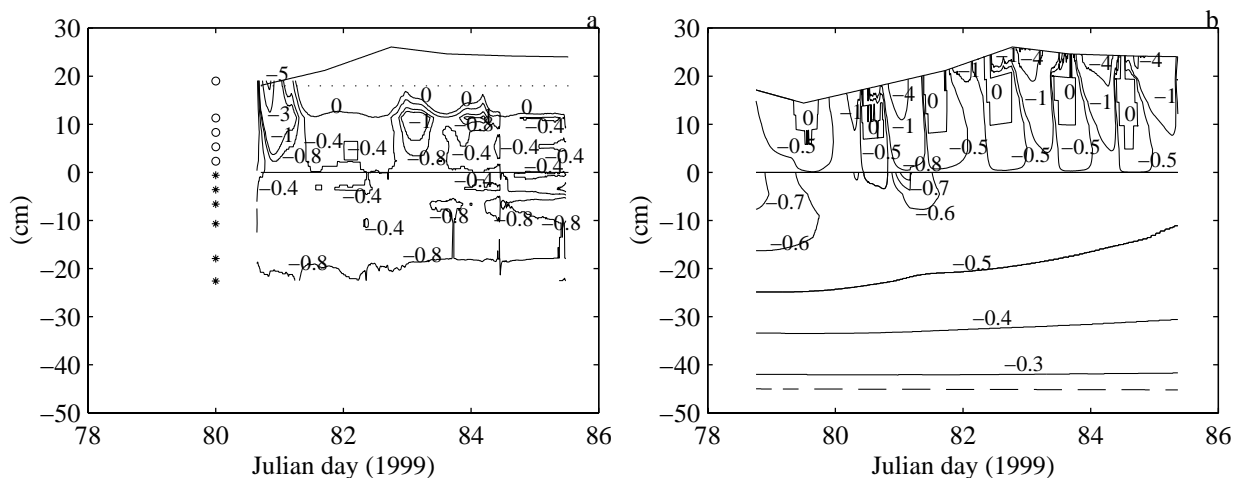

Fig. 8. Snow and ice temperature (°C) during the BASIS-99 experiment. a) Observed snow and ice temperature by thermistor strings. The symbols o and ∗ show the locations of sensors in the snow and ice, respectively. b) Modelled snow and ice temperature.

An analytical solution cannot be obtained for the full ice-physics-based model. Therefore, the effect of numerical resolution is studied by comparisons of intensive numerical model simulations applying various spatial and temporal resolutions. The simulations are made corresponding to the freezing, thermal equilibrium and warm-up (melting) stages of one ice season. The effect of the numerical resolution on model results can be summarized as follows:

During the freezing season, the effect of spatial resolution on the modelled ice growth rate is significant for short-time model runs using a large time step. A large time step should be avoided under conditions of rapid ice growth. For long-period model runs, the ice growth rates become consistent, indicating that the effect of model resolution tends to be diminished.

During the ice thermal equilibrium stage, a low spatial resolution model yields a large diurnal variation in the surface temperature. The amount of solar radiation absorbed in the surface layer tended to complement the surface conductive heat flux. The daily average surface temperature and net surface heat flux were less sensitive to the model spatial resolution. The impact of the spatial resolution on the model results is the greatest near the surface because of the strong gradient in the absorbed solar radiation.

For the warm-up season, the daily minimum surface temperature is sensitive to the spatial resolution. The strongly-attenuated solar radiation absorbed in the surface layer was found to modulate the effect of the grid resolution on the melting. The sub-surface maximum ice temperature can only be simulated with a high spatial resolution model. The model run with a low spatial resolution may damp out the effect of penetrating solar radiation on the ice temperature profile. In late spring when the air temperature is well above freezing point, the ice is warmed from the surface in response to the high air temperature, and the effect of penetrating radiation on model runs using various spatial resolutions tends to be minor.

5.4 Air-ice interaction

5.4.1 The surface heat balance and the turbulent heat fluxes

The surface heat fluxes are of primarily importance in the energy and mass balance of the ice and snow covers. The diurnal variation of short-wave radiation can be estimated quite well, except for some high values that one probably due to multiple reflections between the snow surface and clouds (see, Fig. 4 in paper **III**). The effect of these peaks on the ice ther-

modynamics was, however, minor since their duration was short.

The net long-wave radiation tends to play a key role in the surface heat balance. A number of long-wave radiation schemes were investigated for freezing conditions in paper **II**. According to the inter-comparison between these schemes, the error in the net long-wave radiation can be expected to be some $\pm$ 20 Wm^{-2} for less intensive freezing conditions. The ice model estimates the air-ice turbulent fluxes well on the basis of the Monin-Obukhov similarity theory taking the surface layer stratification into account. In a comparison with measurements made by eddy covariance equipment (sonic anemometer), the average turbulent fluxes estimated by the ice model showed rather good accuracy (Table 2 in paper **III**). Paper **IV** presented some results of turbulence and surface layer characteristics using the BASIS-98 field data. The wind and air temperature measured at 4 levels on a 10 m high weather mast allowed us to apply the gradient method to estimate the surface turbulent fluxes and transfer coefficients. The bulk heat exchange coefficient (C_H) and the temperature roughness length (z_T), which play important roles in the estimation of surface turbulent heat fluxes, were also determined. The aerodynamic roughness length (z_0) was also determined from the field data. An empirical expression between z_0 and z_T and the wind speed was suggested and applied in paper **III** and the model calculations in section 5.2. The turbulent fluxes estimated by the gradient method and the ice model compared reasonably well with the eddy-flux measurements (Fig. 4 in paper **IV**). The surface temperature estimated by the ice model, the gradient method and the eddy flux measurements were mutually in good agreement, indicating a good approximation of the surface heat balance in the ice model.

5.4.2 The coupled air-ice model

During advection of warm air, a large horizontal temperature gradient may occur in the near-surface air above the sea ice cover. There is an interaction between the cooling of the air mass and the heating of the upper layers of snow and/or ice. The magnitude and spatial scale of these heating and cooling processes depend on the meteorological situation, i.e., on the temperature of the air, snow, and ice, on the cloud cover, solar radiation, surface albedo, wind speed, and air humidity as well as on the fetch over the ice. We coupled a two-dimensional mesoscale atmospheric model with our sea ice model to simulate the sea ice thermodynamics during warm-air advection (paper **VI**). Investigations were made of various meteorological conditions with respect to radiative forcing (season and cloud cover effect) and turbulent exchange (wind effect). The coupled

model runs were divided into four groups: (1) springtime with clear skies; (2) springtime with overcast skies; (3) polar night with clear skies and (4) polar night with overcast skies. These were simulated with a wide range of atmospheric pressure gradients, i.e. the geostrophic wind driving the ABL flow, varying from 2 to 24 ms^{-1}.

The ice temperature showed vertical and horizontal redistribution in response to the local surface heat balance, and a horizontal temperature gradient developed in the atmosphere due to the cooling of the air mass. The local surface temperature increases with increasing wind speed. In general, there is a vertical temperature gradient, indicating an upward heat flux through the ice and snow. However, due to the strong surface heating by the turbulent heat flux and the downward long-wave radiation in overcast conditions, the temperature gradient may reverse. The stronger the surface heating the wider was the region where this downward flux occurred. At the downwind edge of this region, the conductive heat flux changed its direction. In model runs under overcast conditions and a light wind, an isothermal layer close to the ice edge can be seen. By increasing the wind speed, a horizontally homogeneous warm snow/ice layer can be generated in the uppermost layers of the whole ice-covered model domain. For model runs under clear sky conditions, the ice temperature regime revealed intensive modification near the ice edge and less modification far from the ice edge. The same effect can also be seen in the model runs under overcast conditions but a low wind speed.

The effects of the warm-air advection on the upper snow and ice layers were most pronounced within a few hours of the beginning of the situation. After this, the heat gradually conducted deeper into the ice, and further from the ice edge the near-surface layers slowly returned towards their undisturbed state of an upward conductive heat flux. In our model runs the diurnal variation of the temperature in the upper snow layers was particularly strong in spring under clear skies and with a light wind. Increasing the wind speed enhanced the turbulent heat fluxes, and thus the relative importance of the solar radiation and the diurnal cycle became smaller.

The development of the stably-stratified atmospheric boundary layer downwind of the ice edge depended above all on the wind speed and cloud cover. A strong wind yields large turbulent fluxes and makes the boundary layer grow deeper. Cloud cover made the ABL warmer.

6 CONCLUSIONS

In this thesis, a one-dimensional thermodynamic sea ice model was constructed with special attention paid to the air-ice interaction and ice thermal varia-

tion. The studies of this thesis dealt with the model physics and numerical mathematics. The model was validated by simulating the ice thermodynamic processes in the Bohai Sea and the Baltic Sea. The numerical scheme of the ice model was evaluated and the impact of the numerical model resolution on model predictions was investigated. The model was coupled with an atmospheric boundary layer model to study the effect of warm air advection on ice thermodynamics and air-ice coupling. The following conclusions were reached:

(1) The sea ice model constructed in this thesis has been proved to be suitable for ice process studies. On the level of formal ice modelling studies, the ice physics is properly considered in the model.

(2) Accurate estimations of surface heat fluxes are necessary in sea ice thermodynamic models, since the ice thermal variation is directly dictated by the surface heat balance. Usually, the ice model can estimate the short-wave radiation well. The inaccuracy in estimation of net long-wave radiation can be expected to reach some $\pm$ 20 Wm^{-2} for less intensive freezing conditions, as determined by inter-comparison of various parameterization schemes. Such a conclusion also roughly agrees with the comparison between the BASIS-98 field measurements and model calculations. The ice model well estimates the air-ice turbulent fluxes based on the Monin-Obukhov similarity theory.

(3) The turbulent transfer coefficients and fluxes during BASIS-98 were accurately determined. The agreement between the gradient-method results and the eddy-correlation results supports the validity of the Monin-Obukhov similarity theory. An empirical expression for the dependence of the scalar roughness length on the aerodynamic roughness length (drag coefficient) and the wind speed was suggested and applied in the ice model. The modelled turbulent fluxes compared rather well with the fluxes from the eddy-correlation and gradient methods.

(4) The model performed well in simulating ice evolution when compared with field observations in the sub-polar ice-covered seas. In the Bohai Sea, the snow layer was thin and had only a minor effect on ice thickness evolution. The modelled ice thickness was in good agreement with the measurements. The modelled ice temperature also compared well with observations.

The ice model yields a good estimate of seasonal ice evolution in the Baltic Sea. For Baltic Sea ice modelling, the snow effect must be taken into account since the snow thickness is significant. The modelling study indicated that a thin layer of newly-fallen snow may theoretically ac-

celerate melting in the spring due to its high volumetric extinction coefficient.

Two-layer parameterization of penetrating solar radiation in sea ice is recommended. An ice model with such a characteristic can reproduce the sub-surface melting which has been widely observed in the field.

High-quality field data serves as a test-bed for process studies. During the ice thermal equilibrium stage, the re-freezing of surface melt water can be regarded as an important factor in the evolution of ice thickness in the Baltic Sea. In early spring, the sub-surface melting contributed significantly to the total melting caused by the penetrating solar radiation. The sub-surface melting is sensitive to the snow's extinction coefficient while the surface melting is sensitive to the snow's thermal properties.

(5) The heat conduction equation of the ice model was solved by a conservative finite-difference scheme based on the integral interpolation method. The scheme was validated by numerical tests and was found to be suitable for the ice model.

(6) Analytical solutions for simplified model conditions were derived and utilized to evaluate the error of the numerical schemes. The results showed that the error decreases exponentially with an increase in model spatial resolution. In the ice growth phase, a large model integral time step should be avoided in order to prevent possible oscillation of the result on a short time-scale. On a short time-scale, such perturbation may ultimately alter the final simulated ice thickness due to its accumulated effect. During the ice thermal equilibrium and the early spring season, the short-wave radiation absorbed within the ice and snow cover was found to modulate the effect of the numerical resolution in the prediction of surface heat flux, ice temperature and surface melting. A model run with a low spatial resolution may damp out the effect of penetrating solar radiation on the ice temperature profile near the surface. This suggests that modelling of the increased sub-surface temperature effect is highly sensitive to the model spatial resolution.

(7) The response of ice/snow to warm air advection was strongly affected by the initial thermal regime of the ice/snow and on the wind speed, the cloud cover and the solar radiation. The ice temperature regime revealed intensive modification near the ice edge. Concurrently, the air mass became colder downwind of the ice edge. From the point of view of the modelling of the atmospheric boundary layer, the model coupling was most important when the wind was strong, because then the modification in the surface temperature was largest. From the point of view of the snow and ice, the coupling was most important when the wind was weak, because then the modification in the air temperature was largest.

Outlook for further studies: The sea ice model constructed in this thesis performed well for ice evolution in the Bohai Sea and the Baltic Sea. However, there are still aspects that need to be studied further. The ice model is primarily constructed for sub-polar ice study. A consideration of the temperature-salinity coupling can extend the model's applications to saline polar sea ice. The surface radiation fluxes can be better estimated by incorporating an atmospheric radiative transfer model. The surface albedo feedback should be better understood. In this model, the ice-ocean interaction is considered simply through Eq. (17) with a fixed oceanic heat flux. Such a first-order parameterization is theoretically simple, but overlooks the details of how oceanic heat flux affects the ice freezing and melting, for which a coupled ice–ocean model would be needed. Most current high-quality meteorological and ice thickness observations have a relative short time-scale (e.g. a few weeks in BASIS-98). For ice process studies, extension of high-quality ice measurement to the seasonal scale may be needed. Presence of liquid water and its effects on the surface heat balance and thermal variation of sea ice need to be further investigated. Further studies analogous to paper **VI** can focus on the importance of the snow cover on the ice, which affects the heat conduction, surface albedo, and the penetration of the solar radiation. Studies on the effect of warm air on the surface mass balance in non-stationary conditions are also relevant, since they often occur in reality.

ACKNOWLEDGMENT

7 REFERENCES

Aagaard, K. & Carmack, E.C. 1989: The role of sea ice and other fresh water in the Arctic circulation. – J. Geophys. Res. 94(C10): 14,485-14,498.

Alestalo, M. & Savijärvi, H. 1985: Mesoscale circulations in a hydrostatic model: coastal convergence and orographic lifting. – Tellus 37A: 156-162.

Anderson, D.L. 1961: Growth rate of sea ice. – J. Glaciol. 3: 1170-1172.

Andreas, E.L. 1987: A theory for the scalar roughness and the scalar transfer coefficients over snow and sea ice. – Boundary-Layer Meteorol. 38: 159-184.

Andreas, E.L. & Ackley, S.F. 1982: On the difference in ablation seasons of Arctic and Antarctic sea ice. – J. Atmos. Sci. 39: 440-447.

Andreas, E. L., Tucker III, W.B. & Ackley, S. F. 1984: Atmospheric boundary-layer modification, drag coefficient and surface heat flux in the Antarctic marginal ice zone. – J. Geophys. Res. 89 (C1): 649-661.

Assur, A. 1958: Composition of sea ice and its tensile strength. – In: Proc. Conf. on Arctic Sea Ice. – Natl. Acad. Sci.-Natl. Res. Council, Washington, D.C., Publ. 598: 106-138.

Ångström, A. 1918: A study of the radiation of the atmosphere. – Smithson. Misc. Collect. 65, 3.

Banke, E.G., Smith, S.D. & Anderson, R.J. 1980: Drag coefficient at AIDJEX from sonic anemometer measurement. – In: Pritchard, R.S. (ed.), Sea Ice Processes and Models. – University of Washington Press, Seattle, pp. 430-442.

Bennett, T.J. 1982: A coupled atmosphere-sea ice model study of the role of sea ice in climatic predictability. – J. Atmos. Sci. 39: 1456-1465.

Bennett, T. J. Jr. & Hunkins, K. 1986: Atmospheric boundary layer modification in the marginal ice zone. – J. Geophys. Res. 91 (C11): 13,033-13,044.

Berljand, M.E. & Berljand, T.G. 1952: Determing the net long-wave radiation of the earth with consideration of the effect of cloudiness. – Izv. Akad. Nauk SSSR Ser. Geofiz., 1: 64-78. (in Russian)

Bitz, C.M. & Lipscomb, W.H. 1999: An energy-conserving thermodynamic model of sea ice. – J. Geophys. Res. 104(C7): 15,669-15,677.

Björk, G. 1992: On the response of the equilibrium thickness distribution of sea ice to ice export, mechanical deformation and thermal forcing with application to the Arctic Ocean. – J. Geophys. Res. 97(C7): 11,287-11,298.

Brandt, R.E. & Warren, S.G. 1993: Solar-heating rates and temperature profiles in Antarctic snow and ice. – J. Glaciol. 39: 99-110.

Brunt, D. 1932: Notes on radiation in the atmosphere. -Q.J.R. Meteorol. Soc. 58: 389-420.

Brustaert, W. 1975: On a derivable formula for long-wave radiation from clear skies. – Water Resour. Res. 11: 742-744.

Brümmer, B., Busack, B. & Hoeber, H. 1994: Boundary-layer observations over water and Arctic sea ice during on-ice air flow. – Boundary-Layer Meteorol. 68: 75-108.

Bøggild, C.E., Winther, J.G., Sand, K. & Elvehøy. H. 1995: Sub-surface melting in blue-ice fields in Dronning Maud Land, Antarctica: Observation and modelling. – Ann. Glaciol. 21: 162-68.

Cheng, B. & Launiainen, J. 1998: A one-dimensional thermodynamic air-ice-water model: technical and algorithm description report. – MERI – Report Series of the Finnish Institute of Marine Research, 37: 15-36.

Cox, G.F.N. & Weeks, W.F. 1974: Salinity variations in sea ice. – J. Glaciol. 13: 109-120.

Cox, G.F.N. & Weeks, W.F. 1988: Numerical simulations of the profile properties of undeformed first-year sea ice during the growth season. – J. Geophys. Res. 93(C10): 12,449-12,460.

Ebert, E.E. & Curry, J.A. 1993: An Intermediate one-dimensional thermodynamic sea ice model for investigating ice-atmosphere interaction. - J. Geophys. Res. 98(C6): 10,085-10,109.

Efimova, N.A. 1961: On methods of calculating monthly values of net long-wave radiation. – Meteorol. Gidrol. 10: 28-33.

Flato, G.M. & Brown, R.D. 1996: Variability and climate sensitivity of landfast Arctic sea ice. – J. Geophys. Res. 101(C10): 25,767-25,777.

Gabison, R. 1987: A thermodynamic model of the formation growth and decay of first-year sea ice. – J. Glaciol. 33: 105-109.

Garratt, J.R. 1992: The atmospheric boundary layer. – Cambridge, Cambridge University Press. – 316 pp.

Grenfell, T.C. 1979: The effects of ice thickness on the exchange of solar radiation over the polar oceans. – J. Glaciol. 22: 305-320.

Grenfell, T.C. & Maykut, G.A. 1977: The optical properties of ice and snow in the Arctic Basin. – J. Glaciol. 18: 445-463.

Guest, P.S. 1998: Surface radiation conditions in the Eastern Weddell Sea during winter. – J. Geophys. Res. 103(C13): 30,761-30,771.

Haapala, J. 2000: Modelling of the seasonal ice cover of the Baltic Sea (Ph. D thesis). – Report series in Geophysics. 42, University of Helsinki, Dept. of Geophysics. – 41 pp.

Haapala, J. & Leppäranta, M. 1996: Simulating the Baltic Sea ice season with a coupled ice-ocean model. – Tellus 48 A: 622-643.

Haapala, J., Alenius, P., Dubra, J., Klyachkin, S.V., Kõuts, T., Leppäranta, M., Omstedt, A., Pakstys, L., Schmelzer, N., Schrum, C., Seinä, A., Strübing, K., Sztobryn, M. & Zaharchenko, E. 1996: IDA, ice data bank for Baltic Sea climate studies. – Report series in Geophysics. 35, University of Helsinki, Dept. of Geophysics. – 45 pp.

Heil, P., Allison, I. & Lytle, V.I. 1996: Seasonal and interannual variations of the oceanic heat flux under a landfast Antarctic sea ice cover. – J. Geophys. Res. 101(C11): 25,741-25,752.

Holtslag, A.A.M. & De Bruin, H.A.R. 1988: Applied modeling of the nighttime surface energy balance over land. – J. Appl. Meteorol. 37: 689-704.

Högström, U. 1988: Non-dimensional wind and temperature profiles in the atmospheric surface layer: A re-evaluation. – Boundary-Layer Meteorol. 42: 55-78.

Idso, S.B. 1981: A set of equations for full spectrum and 8-14 microns and 10.5-12.5 microns thermal radiation from cloudless skies. – Water Resour. Res. 17: 295-304.

Idso, S.B. & Jackson, R.D. 1969: Thermal radiation from the atmosphere. – J. Geophys. Res. 74(23): 5397-5403.

Jacobs, J.D. 1978: Radiation climate of Broughton Island. – In: Barry, R.G. & Jacobs, J.D. (eds), Energy budget studies in relation to fast-ice breakup processes in Davis Strait: climatological overview. – INSTAAR Occasional Paper 26: 105-120. Institute of Arctic and Alpine Research, University of Colorado, Boulder, CO.

Kantha, L. H. & Mellor, G.L. 1989: A numerical model of the atmospheric boundary layer over a marginal ice zone. – J. Geophys. Res. 94(C4): 4959-4970.

Kawamura, T., Shirasawa, K., Ishikawa, N, Lindfors, A., Rasmus, K, Granskog, M.A. Ehn, J., Leppäranta, M., Martma, T. & Vaikmäe, R. 2001: Time-series observations of the structure and properties of brackish ice in the Gulf of Finland. – Ann. of Glaciol. 33: 1-4.

Key, J.R., Silcox, R.A. & Stone, R.S. 1996: Evaluation of surface radiative flux parameterizations for use in sea ice model. – J. Geophys. Res. 101(C2): 3839-3849.

Koh, G. & Jordan, R. 1995: Sub-surface melting in a seasonal snow cover. – J. Glaciol. 41: 474-482.

Kolkki, O. 1969: Katsaus Suomen ilmastoon. [A review on the climate in Finland]. – Ilmatieteen laitoksen tiedonant. 18. – 64 pp. (in Finnish)

Kovacs, A. 1996: Sea ice, Part I. Bulk salinity versus ice floe thickness. – Cold Regions Research and Engineering Laboratory (CRREL) Report 96-7, Hanover, NH. – 16 pp.

Kuzmin, P.P. 1961: Process of snow cover melting. – Gidrometeoizdat, Leningrad (in Russian).

Larkin, B.K. 1964: Some stable explicit difference approximations to the diffusion equation. – Math. Comput., 18: 196-202.

Launiainen, J. 1995: Derivation of the relationship between the Obukhov stability parameter and the bulk Richardson number for the flux-profile studies. – Boundary-Layer Meteorol. 76: 165-179.

Launiainen, J. & Vihma, T. 1990: Derivation of turbulent surface fluxes – an iterative flux-profile method allowing arbitrary observing heights. – Environ. Software. 5: 113-124.

Launiainen, J. & Cheng, B. 1995: A simple non-iterative algorithm for calculating turbulent bulk fluxes in diabatic conditions over water, snow/ice and ground surface. – Report Series in Geophysics, 33, Dept. of Geophysics, University of Helsinki. – 12 pp.

Launiainen, J. (ed), 1999: BALTEX-BASIS Data Report 1998. – International BALTEX secretariat Publication14, Geesthacht, Germany. – 94 pp.

Lemke, P. 1987: A coupled one-dimensional sea ice ocean model. – J. Geophys. Res. 92(C12): 13,164-13,172.

Leppäranta, M. 1981: An ice drift model for the Baltic Sea. – Tellus 33: 583-596.

Leppäranta, M. 1983: A growth model for black ice, snow ice and snow thickness in subarctic basins. – Nordic Hydrol. 14: 59-70.

Leppäranta, M. 1993: A review of analytical models of sea-ice growth. – Atmosphere-Ocean 31(1): 123-138.

Leppäranta, M. & Seinä A. 1982: Statistics of fast ice thickness along the Finnish coast. – Finnish Mar. Res. 249: 62-71.

Leppäranta, M. & Zhang, Z. 1992: A viscous-plastic ice dynamic test model for the Baltic Sea. – Finnish Inst. Marine Res. Internal Report 1992(3). – 14 pp.

Li, R.H. & Feng, G.C. 1980: Numerical solution of differential equation. – Publishers of High Educations, China (in Chinese).

Liston, G.E., Winther, J.G., Bruland, O., Elvehoy, H. & Sand, K. 1999: Below-surface ice melt on the coastal Antarctic ice sheet. – J. Glaciol. 45: 273-285.

Lumb, F.E. 1964: The influence of cloud on hourly amounts of total radiation of the sea surface. – Q.J.R. Meteorol. Soc. 90: 43-56.

Marshunova, M.S. 1966: Principal characteristics of the radiation balance of the underlying surface and the atmosphere in the Arctic. – In: Fletcher, J.O., Keller, B. & Olenicoff, S.M. (eds), Soviet data on the Arctic heat budget and its climate influence. – Memorandum R.M. 5003-PR, Rand Corp., Santa Monica, CA. Pp: 51-131.

Maykut, G.A. 1978: Energy exchange over young sea ice in the central Arctic. – J. Geophys. Res. 83(C7): 3646-2658.

Maykut, G.A. 1982: Large-scale heat exchange and ice production in the central Arctic. – J. Geophys. Res. 87(C10): 7971-7984.

Maykut, G.A. & Untersteiner, N. 1971: Some results from a time dependent thermodynamic model of sea ice. – J. Geophys. Res. 76(6): 1550-1575.

Maykut, G.A. & Church, P.E. 1973: Radiation climate of Barrow, Alaska, 1962-66. – J. Appl. Meteorol. 12: 620-628.

Maykut, G.A. & McPhee, M.G. 1995: Solar heating of the Arctic mixed layer. – J. Geophys. Res. 100(C12): 24,691-24,703.

McPhee, M.G. 1992: Turbulent heat flux in the upper ocean under sea ice. – J. Geophys. Res. 97(C4): 5365-5379.

McPhee, M.G., Ackley, S.F., Guest, P., Huber, B.A., Martinson, D.G., Morison, J.H., Muench, R.D., Padman, L. & Stanton, T.P. 1996: The Antarctic zone flux experiment. Bulletin of the American Meteorological Society. – Vol. 77, No. 6, 1221-1232.

Moritz, R.E. 1978: A model for estimating global solar radiation. – In: Barry, R.G. & Jacobs, J.D. (eds), Energy budget studies in relation to fast-ice breakup processes in Davis Strait: climatological overview. – INSTAAR Occasional Paper 26. 121-142, Institute of Arctic and Alpine Res., Univ. of Colorado, Boulder.

Monin, A.S. & Obukhov, A.M. 1954: Basic turbulent mixing laws in the atmospheric surface layer. – Trudy Geofiz. Inst. Akademii Nauk SSSR 24: 163-187. (in Russian)

Obukhov, A.M. 1946: Turbulence in an atmosphere with a non-uniform temperature. – Trudy Inst. Teoret. Geofiz. Akademii Nauk SSSR. (in Russian) (English translation 1971 in Bound.-Layer Meteorol. 2: 7-29).

Ohmura, A. 1981: Climate and energy balance of the Arctic tundra. – Züricher Geogr. Schr. 3. Geogr. Inst., Zürich, Switzerland. – 448 pp.

Omstedt, A. 1990: A coupled one-dimensional sea ice-ocean model applied to a semi-enclosed basin. – Tellus 42A: 568-582.

Omstedt, A., Nyberg, L. & Leppäranta, M. 1994: A coupled ice-ocean model supporting winter navigation in the Baltic Sea. Part 1: Ice dynamics and water levels. – SMHI reports Oceanography, 17, Norrköping. – 17 pp.

Omstedt, A. & Nyberg, L. 1995: A coupled ice-ocean model supporting winter navigation in the Baltic Sea. Part 2: thermodynamic and meteorological coupling. – SMHI reports Oceanography, 21, Norrköping. – 39 pp.

Omstedt, A. & Wettlaufer, J.S. 1992: Ice growth and oceanic heat flux: models and measurements. – J. Geophys. Res. 97(C6): 9383-9390.

Ono, N. 1968: Thermal properties of sea ice IV. Thermal constants of sea ice. – Low Temp. Sci. Ser. A, 23: 329-349.

Parkinson, C.L. & Washington, W.M. 1979: A large-scale numerical model of sea ice. – J. Geophys. Res. 84(C1): 311-337.

Peixoto, J.P. & Oort, A.H. 1992: Physics of climate. – American Institute of Physics, New York. – 520 pp.

Perovich, D.K. 1991: Seasonal changes in sea ice optical properties during fall freeze-up. – Cold Reg. Sci. Technol. 19: 261-273.

Perovich, D.K. 1996: The optical properties of sea ice. – Cold Regions Research and Engineering Laboratory (CRREL) Report 96-1, Hanover, NH. – 23 pp.

Prata, A.J. 1996: A new long-wave formula for estimating downward clear-sky radiation at the surface. – Q. J. R. Meteorol. Soc. 122: 1127-1151.

Sahlberg, J. 1988: Modelling the thermal regime of a lake during winter season. – Cold Reg. Sci. Technol. 15: 151-159.

Saloranta, T. 2000: Modelling the evolution of snow, snow ice and ice in the Baltic Sea. – Tellus 52A: 93-108.

Saloranta, T.M. 1998: Snow and snow-ice in sea-ice thermodynamic modelling. – Report Series in Geophysics, 39. Dept. of Geophysics, University of Helsinki. – 84 pp.

Satterlund, D.R. 1979: An improved equation for estimating long-wave radiation from the atmosphere. – Water Resour. Res. 15: 1649-1650.

Savijärvi, H. 1997: Diurnal winds around Lake Tanganyika. – Q. J. R. Meteorol. Soc. 123: 901-918.

Schlatter, T.W. 1972: The local surface energy balance and subsurface temperature regimes in Antarctica. – J. Appl. Meteorol. 11(10): 1048-1062.

Schramm, J.L., Holland, M.M., Curry J.A. & Ebert, E.E. 1997: Modelling the thermodynamics of a sea ice thickness distribution. 1. Sensitivity to ice thickness resolution. – J. Geophys. Res. 102(C10): 23,079-23,091.

Schwerdtfeger, P. 1963: The thermal properties of sea ice. – J. Glaciol. 4: 789-807.

Seinä, A., Grönvall, H., Wang, R., Li, Z. & Liu, Q. 1991: Field experiment on fast ice of Bayuquan (Liaodong Bay), Bohai Sea Data report. – Finnish Institute of Marine Research, Internal Report, 1991(1). – 17+15 pp.

Sellers, W.D. 1965: Physical climatology. – Chicago, University of Chicago Press. – 272 pp.

Semtner, A.J. 1976: A model for the thermodynamic growth of sea ice in numerical investigation of climate. – J. Phys. Oceanogr. 6: 379-389.

Shine, K.P. 1984: Parameterization of short wave flux over high albedo surfaces as a function of cloud thickness and surface albedo. – Q. J. R. Meteorol. Soc. 110: 747-764.

Shirasawa, K., Kobinata, K. & Kawamura, T. 2001: Eddy flux measurements below ice and ocean boundary layer studies. – In: Launiainen, J. & Vihma, T. (eds), BALTEX-BASIS Final Report 2001. – International BALTEX Secretariat. Publication 19: 170-178. Geesthacht, Germany.

Simpson, L.S. 1958: Estimation of sea ice formation and growth. – In: Proc. Conf. on Arctic Sea Ice. – Natl. Acad. Sic.-Natl. Res. Council, Washington, D.C., Publ. 598: 162-166.

Stefan, J. 1891: Über die Theorie der Eisbildung, insbesondere über Eisbildung im Polarmeere. – Annln Phys., Band 42, Nr2: 269-286.

Sturm, M., Holmgren, J. König, M. & Morris, K. 1997: The thermal conductivity of seasonal snow. – J. Glaciol. 43: 26-40.

Swinbank, W.C. 1963: Longwave radiation from clear skies. – Q. J. R. Meteorol. Soc. 89: 339-348.

Udin, I. & Ullerstig, A. 1976: A numerical model for forecasting the ice motion in the Bay and Sea of Bothnia. – Winter Navigation Research Board, Swedish Administration of Shipping and Navigation, Finnish Board of Navigation. Research report 18. – 40 pp.

Untersteiner, N. 1961: On the mass and heat budget of Arctic sea ice. – Arch. Meteorol. Geophys. Bioklimatol. A, 12: 151-182.

Untersteiner, N. 1964: Calculations of temperature regime and heat budget of sea ice in the central Arctic. – J. Geophys. Res. 69(22): 4755-4766.

Vihma, T. 1995. Subgrid parameterization of surface heat and momentum fluxes over polar oceans. – J. Geophys. Res. 100(11): 22,625-22,646.

Vihma, T., Uotila, J., Cheng, B., Purokoski, T., Kosloff, P., Launiainen, J. & Schrum, C. 1999: Marine meteorological sea ice and oceanographic observation by the Finnish Institute of Marine Research. – In: Launiainen, J. (ed.), BALTEX-BASIS Data Report 1998. – International BALTEX secretariat. Publication14: 14-25. Geesthacht, Germany.

Vihma, T. & Brümmer, B. 2002: Observations and modelling of on-ice and off-ice flows in the northern Baltic Sea. – Boundary-Layer Meteorol. 103(1): 1-27.

Vihma, T., Uotila, J., Cheng, B. & Launiainen, J. 2002: Surface heat budget over the Weddell Sea: Buoy results and comparisons with large-scale models. – J. Geophys. Res. 107(C2). (in press)

Wang, Z. & Wu, H. 1994: Sea ice thermal processes and simulation of their coupling with the dynamic process. – Oceanologia et Limnologia Sinica. 25 (4): 408-415. (in Chinese)

Wang, K., Bai, S. & Wu, H. 1999: Parameterization of sea ice thermodynamic process. – Marine Forecasts. 16(3): 104-133. (in Chinese)

Weeks, W.F. & Ackley, S.F. 1986: The growth, structure, and properties of sea ice. – In: Untersteiner, N. (ed.), The geophysics of sea ice. – Plenum Press, New York, pp. 9-164.

Weeks, W.F. Gow, A.J., Kosloff, P. & Digby-Argus, S. 1990: The internal structure, composition and properties of brackish ice from the Bay of Bothnia. – In: Ackley, S.F. & Weeks, W.F. (eds), Sea ice properties and processes. – Proceedings of the W.F. Weeks Sea Ice Symposium, Cold Regions Research and Engineering Laboratory (CRREL) Monograph 90-1: 1-15.

Wettlaufer, J.S., Untersteiner, N. & Colony, R. 1990: Estimating oceanic heat flux from sea-ice thickness and temperature data. – Ann. Glaciol. 14: 315-318.

Winther, J.G., Elvehoy, H., Boggild, C.E., Sand, K. & Liston, G. 1996: Melting, runoff and the formation of frozen lakes in a mixed snow and blue-ice field in Dronning Maud Land, Antarctica. – J. Glaciol. 42: 271-278.

Winton, M. 2000: A reformulated three-layer sea ice model. – Journal of Atmospheric and Ocean Technology 17: 525-531.

Wu, H. & Leppäranta, M. 1988: On the modelling of ice drift in the Bohai Sea. – Finnish Inst. Marine Res. Internal Report 1988(1). – 40 pp.

Wu, H., Bai, S. Zhang, Z. & Li, G. 1997: Numerical simulation for dynamical processes of sea ice. – Acta Oceanologica Sinica. 16(3): 303-325.

Wu, H., Bai, S. & Zhang, Z. 1998: Numerical sea ice prediction in China. – Acta Oceanologica Sinica. 17(2): 167-185.

Yen, Y.-C. 1981: Review of thermal properties of snow, ice and sea ice. – Cold Regions Research and Engineering Laboratory (CRREL) Report 81-10, Hanover, NH. – 26 pp.

Zillman, J.W. 1972: A study of some aspects of the radiation and heat budgets of the southern hemisphere oceans. – Meteorol. Stud. Rep. 26, Bur. of Meteorol., Dep. of the Inter., Canberra, A.C.T.

Zhang, Z. 2000: On modelling ice dynamics of semi-enclosed seasonally ice-covered seas (Ph.D thesis). – Report series in Geophysics 43, University of Helsinki, Dept. of Geophysics. – 33 pp.

Appendix: A numerical scheme with an uneven spatial grid size derived by the numerical integral interpolation method

Paper **I** and appendix B in paper **II** introduced the numerical integral interpolation method and a numerical scheme with equal sparial grid size was derived. Here, we present a example of how to use this method to derive a scheme with an uneven spatial grid size. The procedure illustrated that no distinct extra work are needed to obtain such a flexible scheme compared with work done in papers **I** and **II**. This is one merit of the numerical integral interpolation method.

The heat conduction equation (1) can be re-written in a compact form:

$$(\rho c)\frac{\partial T(z,t)}{\partial t}=\frac{\partial}{\partial z}\left(k\frac{\partial T(z,t)}{\partial z}\right)-F(z,t) \tag{a1}$$

where $(\rho c) = \rho c(z,t)$, $k = k(z,t)$ and $F(z,t) = \partial q(z,t)/\partial z$. The numerical integration has been made for each term in (a1) with respect to an area in z,t space defined by $[z_{j-1/2}, z_{j+1/2}]$ and $[t_k, t_{k+1}]$; see Figure A, where $j = 1, 2,...N$ denote the inner grid points in ice, with the corresponding grid size being $h_1, h_2,...h_N$. The integral time step is $T_{k+1}-T_k = \tau$

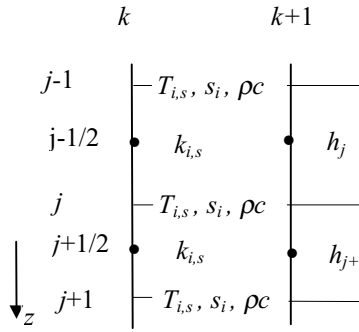Figure A. Numerical integration of Eq. (a1) with an uneven vertical grid ($h_j \neq h_{j+1}$) definition. The variables (ρ, c, k, s, T) on grid system is staggered.

According to the intermediate value theorem of integration, the first term of (a1) becomes

$$\int_{z_{j-1/2}}^{z_{j+1/2}}\int_{t_k}^{t_{k+1}}\rho c\frac{\partial T}{\partial t}dzdt\approx\int_{z_{j-1/2}}^{z_{j+1/2}}\rho c(z_j,t_k)\cdot T(z,t_{k+1})dz-\int_{z_{j-1/2}}^{z_{j+1/2}}\rho c(z_j,t_k)\cdot T(z,t_k)dz$$

Applying the integral approximation, e.g. the central rectangle formula, we have:

$$\int_{z_{j-1/2}}^{z_{j+1/2}}\rho c(z_j,t_k)\cdot T(z_j,t_{k+1})dz\approx\frac{h_j+h_{j+1}}{2}\rho c(z_j,t_k)\cdot T_j^{k+1} \text{ , and}$$

$$\int_{z_{j-1/2}}^{z_{j+1/2}}\rho c(z_j,t_k)\cdot T(z_j,t_k)dz\approx\frac{h_j+h_{j+1}}{2}\rho c(z_j,t_k)\cdot T_j^{k}$$

As to the second item in (a1), by assuming $X=k\frac{\partial T(z,t)}{\partial z}$, thus $\frac{\partial T(z,t)}{\partial z}=\frac{X}{k}$ and integrating between $[z_j, z_{j+1}]$ and $[z_{j-1}, z_j]$, we have

$$T(z_{j+1},t)-T(z_j,t)=\int_{z_j}^{z_{j+1}}\frac{X(z,t)}{k}dz\approx X(z_{j+1/2},t)\int_{z_j}^{z_{j+1}}\frac{1}{k}dz \text{ and}$$

$$T(z_j,t)-T(z_{j-1},t)=\int_{z_{j-1}}^{z_j}\frac{X(z,t)}{k}dz\approx X(z_{j-1/2},t)\int_{z_{j-1}}^{z_j}\frac{1}{k}dz$$

With mathematical transformations, and using the central rectangle formula of numerical integral approximation, we have:

$$X(z_{j+1/2},t) \approx \frac{T(z_{j+1},t)-T(z_j,t)}{h_{j+1}}a_{j+1}^t \text{ and } X(z_{j-1/2},t) \approx \frac{T(z_j,t)-T(z_{j-1},t)}{h_j}a_j^t$$

where $a_{j+1}^t = h_{j+1}\left(\int_{z_j}^{z_{j+1}}\frac{1}{k}dz\right)^{-1} \approx k(z_{j+1/2},t)$ and, $a_j^t = h_j\left(\int_{z_{j-1}}^{z_j}\frac{1}{k}dz\right)^{-1} \approx k(z_{j-1/2},t)$, respectively.

Integrating now the second item in (a1) over the area of $[z_{j-1/2},z_{j+1/2}]$ and $[t_k,t_{k+1}]$, we have

$$\int_{z_{j-1/2}}^{z_{j+1/2}}\int_{t_k}^{t_{k+1}}\frac{\partial X}{\partial z}dzdt = \int_{t_k}^{t_{k+1}}\left[X(z_{j+1/2},t)-X(z_{j-1/2},t)\right]dt$$

We apply an approximate calculation to the right side, so that:

$$\int_{t_k}^{t_{k+1}}X(z_{j+1/2},t)dt \approx \tau\theta\cdot X(z_{j+1/2},t_{k+1})+\tau(1-\theta)\cdot X(z_{j+1/2},t_k) \text{ and}$$

$$\int_{t_k}^{t_{k+1}}X(z_{j-1/2},t)dt \approx \tau\theta\cdot X(z_{j-1/2},t_{k+1})+\tau(1-\theta)\cdot X(z_{j-1/2},t_k) \text{ in which } 0\leq\theta\leq1$$

Numerical integration of the third item in (a1) with an approximate calculation leads to:

$$\int_{z_{j-1/2}}^{z_{j+1/2}}\int_{t_k}^{t_{k+1}}F(z,t)dzdt \approx \tau\cdot\frac{1}{2}(h_j+h_{j+1})F_{z_j}^{t_{k+1/2}}$$

Incorporating these results in the form of integration of (a1), and making the proper mathematical transformations, we finally obtain the numerical scheme of (a1) as

$$-\frac{\tau\theta}{h_j}a_j^{k+1}T_{j-1}^{k+1}+\left[\frac{h_j+h_{j+1}}{2}\rho c_j^{\ k}+\tau\theta\left(\frac{a_{j+1}^{k+1}}{h_{j+1}}+\frac{a_j^{k+1}}{h_j}\right)\right]T_j^{k+1}-\frac{\tau\theta}{h_{j+1}}a_{j+1}^{k+1}T_{j+1}^{k+1}$$

$$=\frac{\tau(1-\theta)}{h_j}a_j^kT_{j-1}^k+\left[\frac{h_j+h_{j+1}}{2}\rho c_j^{\ k}-\tau(1-\theta)\cdot\left(\frac{a_{j+1}^k}{h_{j+1}}+\frac{a_j^k}{h_j}\right)\right]T_j^k+\frac{\tau(1-\theta)}{h_{j+1}}a_{j+1}^kT_{j+1}^k+\frac{\tau}{2}(h_j+h_{j+1})F_j^{k+1/2}$$

$$j=1,2,..\ N \tag{a2}$$

The in-ice temperature can be solved by this matrix system using the speed-up method, once the initial and boundary conditions are given. Following the parameterizations of ice thermal properties given by Maykut & Untersteiner (1971), the $\rho c_j^{\ k}$ may be estimated by $(\rho c)_0+\frac{\gamma\cdot s_j}{(T_j^k-273)^2}$ where s_j and T_j^k are the ice salinity and temperature respectively at grid point j. The $a_{j+1}^t \approx k(z_{j+1/2},t)$ may be estimated by $\frac{(k_{j+1}^k+k_j^k)}{2}=k_0+\frac{\beta\cdot s_j}{2}\left(\frac{1}{(T_{j+1}^k-273)}+\frac{1}{(T_j^k-273)}\right)$ or $k(z_{j+1/2},t)=k_0+\frac{\beta\cdot s_{j+1/2}}{(T_{j+1}^k+T_j^k)/2-273}$. The $F_j^{k+1/2}$ can easily be calculated by its parameterization scheme.